Inorganic Chemistry

Article

pubs.acs.org/IC

Zirconium(IV)−Benzene Phosphonate Coordination Polymers: Lanthanide and Actinide Extraction and Thermal Properties

Vittorio Luca,*[,†] Juan J. Tejada,[†] Daniel Vega,[†] Guilhem Arrachart,[‡] and Cyrielle Rey[‡]

[†]Comisión Nacional de Energía Atómica, Centro Atómico Constituyentes, Avenida General Paz 1499, San Martin 1650, Buenos Aires, Argentina

[‡]Institut de Chimie Séparative de Marcoule, ICSM UMR 5257, CEA-CNRS-UM-ENSCM, Site de Marcoule, Bâtiment 426 BP 17171, F-30207 Bagnols sur Cèze, France

Supporting Information

ABSTRACT: Coordination polymers with different P/(Zr + P) molar ratios were prepared by combining aqueous solutions of Zr(IV) and benzenephosphonate derivatives. 1,3,5-Benzenetrisphosphonic acid (BTP) as well as phosphonocarboxylate derivatives in which carboxylate substitutes one or two of the phosphonate groups were chosen as the building blocks. The precipitates obtained on combining the two solutions were not X-ray amorphous but rather were indicative of poorly ordered materials. Hydrothermal treatment did not alter the structure of the materials produced but did result in improved crystalline order. The use of HF as a mineralizing agent during hydrothermal synthesis resulted in the crystallization of at least three relatively crystalline phases whose structure could not be determined owing to the complexity of the diffraction patterns. Gauging from the similarity of the diffraction patterns of all the phases, the poorly ordered precipitates and crystalline materials appeared to have similar underlying structures. The BTP-based zirconium phosphonates all showed a higher selectivity for lanthanides and thorium compared with cations such as Cs^{+}, Sr^{2+}, and Co^{2+}. Substitution of phosphonate groups by carboxylate groups did little to alter the pattern of selectivity implying that selectivity in the system was entirely determined by the −POH group with little influence from the −COOH groups. Samples with the highest phosphorus content showed the highest extraction efficiencies for lanthanide elements, especially the heavy lanthanides such as Dy^{3+} and Ho^{3+} with separation factors of around four with respect to La^{3+}. In highly acid solutions (4 M HNO_3) there was a pronounced variation in extraction efficiency across the lanthanide series. In situ, nonambient diffraction was performed on ZrBTP-0.8 loaded with Th, Ce, and a complex mixture of lanthanides. In all cases the crystalline $Zr_2P_2O_7$ pyrophosphate phase was formed at ∼800 °C demonstrating the versatility of this structure.

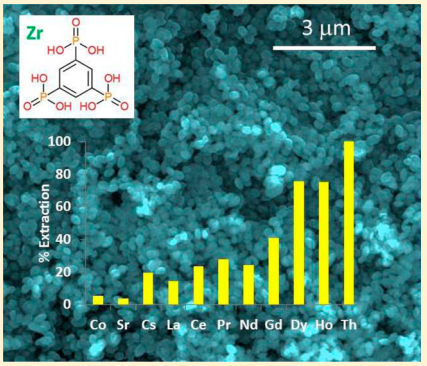

1. INTRODUCTION

The separation or partitioning of trivalent lanthanides from trivalent minor actinides and subsequent transmutation of the latter in fast reactors represents an important option in the move to a more sustainable fuel cycle for nuclear fission energy, since the potential benefits are reduced repository heat load and improved energy utilization[1] as well as greatly reduced long-term waste radiotoxicity.[2]

The major approaches for the separation of trivalent minor actinides from other fission product isotopes have been liquid−liquid extraction, otherwise known as solvent-extraction, and pyroelectrochemical separations.[2,3] Even though the latter is a dry process not involving the use of solvents, it is the former that is at a more advanced stage of development and deployment. Solid-phase extraction is an alternative to liquid−liquid extraction that in relative terms has been little contemplated. It has the advantage of not requiring the organic solvents that represent a significant fire/explosion hazard within nuclear installations and not having to deal with third-phase formation that is another undesirable aspect of solvent-extraction along with the need to manage the decomposition of solvents and extractants. Furthermore, the deployment of solid-phase extraction technologies is straightforward compared with liquid−liquid extraction.

Because of the similarity of their chemistry the trivalent lanthanides and minor actinides are notoriously difficult to separate. For the same reasons intralanthanide extractions are also difficult to accomplish and often require hundreds of laborious extraction cycles.[4] Since the predominant oxidation state of lanthanides and minor actinides is generally three under environmental conditions they are classified according to Pearson as hard ions. They are thus most likely to form strong complexes with hard ligands containing highly electronegative elements such as F^{-}, SO_4^{2-}, CO_3^{2-}, PO_4^{3-}, and OH^{-}.[5] Organophosphorus reagents such as TBP, DTPA, CMPO, and 2-ethylhexyl phosphoric acid (HDEHP) are therefore among the most useful extractants in solvent extraction systems and form the basis of many solvent extraction processes for the separation of lanthanides from actinides.[6−9]

Received: April 17, 2016

ACS Publications © XXXX American Chemical Society

DOI: 10.1021/acs.inorgchem.6b00954
Inorg. Chem. XXXX, XXX, XXX−XXX

The key element of a solid-phase extraction technology is the selectivity of the solid-phase extractant for the target elements or radionuclides. The literature is indeed replete with descriptions of interesting solid materials with potentially interesting adsorption properties, although relatively few of these have been studied in great detail. For instance, extensive commercial use is made of porous materials such as zeolites for applications in the extraction of heavy metal ions and the separation and storage of gases as well as in catalysis. Zeolite-like mixed-coordination silicotitanates and related materials have applications for the selective adsorption of radio cesium.[10,11] Functionalized mesoporous metal oxides prepared by anchoring of organic molecules such as organosilanes and organophosphonates to the surfaces of mesoporous materials prepared through supramolecular self-assembly offer considerable tailorability, since there is scope to vary both the organic and inorganic component and the porosity of the oxide. The use of high surface area supports is generally considered a means of maximizing the number of surface active sites and therefore capacity. Indeed our group and others have shown considerable potential of such functionalized mesoporous oxides for the adsorption of lanthanides and actinides.[12−20] One of the limitations of such functionalized mesoporous oxide materials, however, is the potential fragility of the coupling between metal oxide and the functional organic group. Another limitation is the fact that the loading of functional organic groups on the preassembled metal oxide is generally low, hence, compromising the capacity of the adsorbent. The coassembly of a functional open framework metal oxide in the presence of surfactants is an approach that can be realized in one pot and has the potential to achieve higher loading of organic. Such coassembly or direct synthesis has been undertaken and extensively reported in the case of functionalized mesoporous materials.[21]

Extraction chromatographic resins, or solvent impregnated resins as they are sometimes also called, are similar to the functionalized mesoporous materials in the sense that an extract molecule (that is generally not miscible with water) is incorporated within a porous host substrate.[22] In this case macroreticular polymeric resins have been the popular choice, and the incorporation of the extractant molecules usually occurs via impregnation utilizing a suitable solvent. Since the extractant molecule is not covalently bound within the matrix there is scope for it to be leached.[23] Such extraction chromatographic resins containing organophosphorus reagents have shown utility for small scale analytical applications.[24−26]

Yet another class of materials that has seen significant interest in more recent times consists of the coordination polymers that result from the coordination of metal cations by multifunctional organic ligands to form compounds that extend continuously in one, two, and three dimensions as in the case of metal organic frameworks (MOFs).[27] MOFs generally have ordered three-dimensional porous structures, and while the vast majority of reported coordination polymers and MOFs are macroscopic crystalline materials, they can also be amorphous.[28] The hexacyannoferrates can be regarded as traditional members of the coordination polymer family, and their ion-exchange properties are well-documented and have been extensively explored. That the couplings of group IV metal cations and organic moieties can yield polymer-like porous materials was demonstrated by Clearfield and others as early as the mid-1990s.[29,30] Nowadays the one-step hydrothermal reaction between reactive metals or organometallic precursors and complexing polyfunctional organic molecules with or without the use of a template to form a coordination polymer network is yielding an ever-expanding array of new and exciting compounds.[31] If these coordination polymers consist of crystalline open frameworks then they are known as MOFs. Like mesoporous metal oxides generated through supramolecular self-assembly, MOFs can have enormous surface areas. Their utility for the adsorption and separation of gases is being studied intensively, and impressive capacities and selectivities for different gases have been demonstrated.

Given the aforementioned affinity between phosphonate ligands and trivalent lanthanides and actinides it is natural to consider the use of coordination polymers involving organophosphorus ligands possessing multiple binding sites. Indeed group (IV) metal organophosphonates based on the α-zirconium phosphate motif have been extensively studied for many decades and have shown utility for the separation of lanthanides and actinides.[32−34] Particularly attractive are the compounds generated with Zr(IV), since they are highly insoluble in both acidic and alkaline solutions. Of the thousands of coordination polymers and MOFs that have been prepared to date, only relatively few involve the coupling of Zr(IV) with phosphonate ligands to give highly insoluble compounds.[35−38] Insofar as the ability of such compounds to extract actinides is concerned, such materials have only relatively recently begun to be studied. For instance, Carboni et al. studied the adsorption of UO_2^{2+} on UiO MOFs at a pH of 2.5.[39]

We recently focused our attention[40] on the development of coordination polymers prepared through the coordination of Zr(IV) to the trisphosphonic acid amino trismethylene phosphonate (ATMP) under hydrothermal conditions. These X-ray amorphous materials showed very high affinities for the trivalent lanthanides and interesting intralanthanide separation factors. Intralanthanide separations are increasing in importance owing to the desire to utilize various lanthanides in advanced technologies.

Subsequently we reported on the preparation and extraction properties of similarly amorphous compounds formed between zirconium(IV) and [1-hydroxy-2-(1*H*-imidazol-1-yl)ethane-1,1-diyl]bis(phosphonic acid) (zoledronic acid).[41] These zirconium-zoledronate coordination polymers displayed surprisingly similar selectivities to the zirconium-ATMP compounds despite the inclusion of the imidazolate functionality. Additionally, certain compositions were shown to have excellent capability for separating the actinide thorium from complex mixtures of lanthanides, actinides, and fission product elements particularly when granulated with polyacrylonitrile. The quantitative extraction of thorium from a complex mixture or lanthanide elements could have important implications in rare earth minerals processing as it can be an important radioactive contaminant.[42]

It was also demonstrated that the zirconium-zoledronate coordination polymers, once loaded with an actinide, could also easily be converted to phosphate ceramics with the NZP structure that are known as highly durable host phases for actinides. Such a cradle-to-grave strategy has been discussed as long ago as the 1970s[43] and has been applied in relation to the use of crystalline silicotitanates, where it was demonstrated that highly Cs-selective inorganic ion exchangers could be converted directly into stable pollucite ceramics[44] and mesoporous zirconium titanates.[14]

In the present contribution we explored the possibility of coupling zirconium(IV) to 1,3,5-benzene trisphosphonic acid

DOI: 10.1021/acs.inorgchem.6b00954
Inorg. Chem. XXXX, XXX, XXX−XXX

(BTP) ligands and ligands in which the 1,3,5-trisubstituted benzene ring carboxylic acid functions systematically replace one (BDP) or two (BMP) of phosphonic acid groups. Such a replacement in addition to structural nuances might be expected to modulate the basicity of P═O groups and the acidity of P(O)OH protons as well as impose steric effects such as to influence metal ion extraction efficiency.[26] The rigidity of the 1,3,5-trisubstituted benzene could yield framework structures that would have greater structural order as well as higher thermal and chemical stability than achievable with more flexible ligands.

2. EXPERIMENTAL SECTION

2.1. Synthesis of Benzene Phosphonates. 1,3,5-Trisubstituted benzene ring with one phosphonic and two carboxylic acid groups (**BMP**: Benzene MonoPhosphonic acid); two phosphonic and one carboxylic acid groups (**BDP**: Benzene DiPhosphonic acid); or three phosphonic acid group (**BTP**: Benzene TriPhosphonic acid) were obtained by a catalytic Arbusov reaction from the corresponding bromide compound and triethyl phosphite in the presence of nickel(II) bromide followed by a hydrolysis reaction of the methyl carboxylate and phosphonate groups. See reaction scheme in the Supporting Information section.

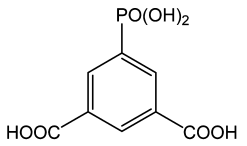

5-phosphonoisophthalic acid
BMP(Benzene MonoPhosphonic acid)

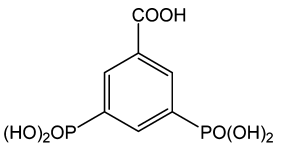

3,5-diphosphonobenzoic acid
BDP (Benzene DiPhosphonic acid)

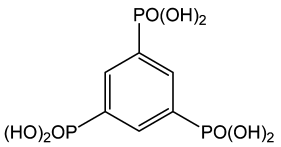

benzene-1,3,5-tris(phosphonic acid)
BTP (Benzene TriPhosphonic acid)

5-Bromoisophthalic acid was treated by thionyl chloride and a methanolic solution to provide dimethyl 5-bromoisophthalate, which was then engaged in a catalytic Arbusov reaction. The resulting dimethyl 5-(diethoxyphosphoryl)isophthalate compound was treated by a hydrochloric acid solution (HCl 20%) providing the 5-phosphonoisophthalic acid, which was called **BMP**.

3,5-Dibromobenzoic acid was treated by thionyl chloride and a methanolic solution to provide methyl 3,5-dibromobenzoate, which was then engaged in a catalytic Arbusov reaction. The resulting methyl 3,5-bis(diethoxyphosphoryl)benzoate compound is treated by a hydrochloric acid solution (HCl 20%) providing the 3,5-diphosphonobenzoic acid, which was called **BDP**.

1,3,5-Tribromobenzene was engaged in a catalytic Arbusov reaction providing the hexaethylbenzene-1,3,5-tris(phosphonate) compound, which was treated by a hydrochloric acid solution (HCl 20%) yielding the benzene-1,3,5-tri(phosphonic) acid, which was called **BTP**.

2.2. General Procedure for Benzoate Compounds. A solution of 3,5-dibromobenzoic acid or 5-bromoisophthalic acid (30 mmol) in $SOCl_2$ (10−15 mL) was refluxed for 5 h under nitrogen atmosphere. Excess $SOCl_2$ was removed under reduced pressure, and then the residue was refluxed in methanol (10−15 mL) for 12 h. The solvent was evaporated, and the residue was filtrated and washed by methanol to afford in a quantitative yield the final compounds as white solids.

Dimethyl 5-Bromoisophthalate. ^{1}H NMR (400 MHz, $CDCl_3$): δ(ppm) 8.4(s, 2H$_{ar}$), 8.18 (s, 2H$_{ar}$), 3.96 (s, 6H, CH_3); ^{13}C NMR (100 MHz, $CDCl_3$): δ(ppm) 165.1 (C═O), 136.3−122.9 (C$_{ar}$), 51.5 (CH_3).

Methyl 3,5-Bromobenzoate. ^{1}H NMR (400 MHz, $CDCl_3$): δ(ppm) 8.12 (d, 2H$_{ar}$), 7.87 (t, 1H$_{ar}$), 3.95 (s, 3H, CH_3); ^{13}C NMR (100 MHz, $CDCl_3$): δ(ppm) 164.5 (C═O), 138.3−123.1 (C$_{ar}$), 52.8 (CH_3).

2.3. General Procedure for Arbusov Reaction. The Arbusov reaction was performed using an adapted literature protocol.[45] Briefly, a suspension of appropriate bromo derivatives (dimethyl 5-bromoisophthalate; methyl 3,5-bromobenzoate, or 1,3,5-tribromobenzene) (8−20 mmol) in 1,3-diisopropylbenzene (20−50 mL) was heated to 180 °C for 15 min under nitrogen allowing the solubilization of the bromo derivatives. The solution was cooled to room temperature, and nickel(II) bromide (2−5 mmol) was added under nitrogen. The reaction mixture was heated to 180 °C, and triethyl phosphite (30−90 mmol) was added dropwise over 8 h. The resulting mixture was maintained overnight under reflux, under nitrogen. Excess of triethyl phosphite and the 1,3-diisopropylbenzene was distilled off under reduced pressure. The residues were then purified by flash chromatography on silica gel using CH_2Cl_2 as eluent, followed by CH_2Cl_2/CH_3OH (95/5).

Dimethyl 5-(Diethoxyphosphoryl)isophthalate. ^{1}H NMR (400 MHz, $CDCl_3$): δ(ppm) 8.77 (s, 1H$_{ar}$), 8.56−8.59(d, 2H$_{ar}$), 4.09 (m, 4H, CH_2O), 4.05 (s, 6H, CH_3O), 1.28 (t, 6H, CH_3); ^{13}C NMR (100 MHz, $CDCl_3$): δ(ppm) 165.3 (C═O), 136.8−129.4 (C$_{ar}$), 62.6 (CH_2O), 52.6 (CH_3O), 16.3(CH_3); ^{31}P NMR (162 MHz, $CDCl_3$): δ(ppm) 15.65.

Methyl 3,5-Bis(diethoxyphosphoryl)benzoate. ^{1}H NMR (400 MHz, $CDCl_3$): δ(ppm) 8.59 (d, 2H$_{ar}$), 8.39(M, 1H$_{ar}$), 4.14 (m, 8H, CH_2O), 3.95 (s, 3H, CH_3O), 1.32 (t, 12H, CH_3); ^{13}C NMR (100 MHz, $CDCl_3$): δ(ppm) 165.3 (C═O), 138.7−129.3 (C$_{ar}$), 62.6 (CH_2O), 52.6 (CH_3O), 16.3(CH_3); ^{31}P NMR (162 MHz, $CDCl_3$): δ(ppm) 15.44.

Hexaethylbenzene-1,3,5-tris(phosphonate). ^{1}H NMR (400 MHz, $CDCl_3$): δ(ppm) 8.38(m, 3H$_{ar}$), 4.15 (m, 12H, CH_2O), 1.33 (t, 24H, CH_3); ^{13}C NMR (100 MHz, $CDCl_3$): δ(ppm) 138.3−129.7 (C$_{ar}$), 62.6 (CH_2O), 16.3(CH_3); ^{31}P NMR (162 MHz, $CDCl_3$): δ(ppm) 15.32.

2.4. General Procedure for Hydrolysis Reaction. A suspension of appropriate phosphonate derivatives (dimethyl 5-(diethoxyphosphoryl)isophthalate, methyl 3,5-bis(diethoxyphosphoryl)benzoate, or hexaethylbenzene-1,3,5-tris(phosphonate) (15 mmol) in hydrochloric acid solution (20%, 50 mL) were refluxed for 12 h. The acidic solution was evaporated dryness under reduced pressure. Then the residue was dissolved in a minimum of distilled water, and freeze-drying afforded final compounds as solid.

5-Phosphonoisophthalic Acid: Benzene Monophosphonic Acid). ^{1}H NMR (400 MHz, D_2O): δ(ppm) 8.43(s, 1H$_{ar}$), 8.35−8.31(d, 2H$_{ar}$); ^{13}C NMR (100 MHz, D_2O): δ(ppm) 168.4 (C═O), 135.8-130.3(C$_{ar}$); ^{31}P NMR (162 MHz, D_2O): δ(ppm) 11.88. HRMS (ESI-) Calcd. Mass for $C_8H_6O_7P$: 244.9851, Found 244.9854.

3,5-Diphosphonobenzoic Acid: Benzene Diphosphonic Acid). ^{1}H NMR (400 MHz, D_2O): δ(ppm) 8.40(m, 2H$_{ar}$), 8.22(t, 1H$_{ar}$); ^{13}C NMR (100 MHz, D_2O): δ(ppm) 169.1 (C═O), 136.6−130.2(C$_{ar}$); ^{31}P NMR (162 MHz, D_2O): δ(ppm) 12.27. HRMS (ESI-) Calcd. Mass for $C_7H_7O_8P_2$: 280.16, Found 280.9619.

Benzene-1,3,5-tri(phosphonic acid): Benzene Triphosphonic Acid). ^{1}H NMR (400 MHz, D_2O): δ(ppm) 8.11(m, 3H$_{ar}$); ^{13}C NMR (100 MHz, D_2O): δ(ppm) 135.2- 132.2(C$_{ar}$); ^{31}P NMR (162 MHz, D_2O): δ(ppm) 12.94. HRMS (ESI-) Calcd. Mass for $C_6H_8O_9P_3$: 316.9381, Found 316.9363.

2.5. Synthesis of Zr(IV)-Benzene Phosphonate Compounds. The coordination polymers were prepared by first dissolving the benzene phosphonate (BMP, BDP, or BTP) in water using a magnetic stirrer. In some cases 4 M HNO_3 or hydrofluoric acid was added to the stirred BMP, BDP, or BTP solution. Once the dissolution was complete, an appropriate volume of 0.5 M $ZrOCl_2{\cdot}8H_2O$ solution was added while stirring thoroughly. The mixture was then loaded into a polytetrafluoroethylene-lined autoclave, which was heated in a fan-forced oven up to ∼160 °C for several days. At the end of the reaction the autoclave was quenched, and the product was isolated by filtration followed by washing with milli-Q water. In addition to using water as the solvent, numerous materials with variable phosphorus mole

DOI: 10.1021/acs.inorgchem.6b00954
Inorg. Chem. XXXX, XXX, XXX−XXX

fractions were also prepared in tetrahydrofuran and EtOH. These materials are being referred to as generation I (Gen I). A series of compounds was synthesized hydrothermally using a fixed P/(Zr + P) mole ratio but with variable amounts of HF. The HF was used to mineralize the Zr and ensure it remains in solution during the hydrothermal reaction. These materials with variable F/Zr molar ratio are called generation II (Gen II) and generation III (Gen III) for the more crystalline materials.

Granulation of the Zr phosphonates was achieved as previously described.[16] Briefly, to a 6 wt % solution of polyacrylonitrile (PAN) in dimethyl sulfoxide (DMSO) was added sufficient ZrBTP-x to give a 60 wt % loading of the compound in PAN. The solid was dispersed in the PAN-DMSO solution by agitation and sonication until a smooth slurry was obtained. Beads were generated by adding droplets of the solution to a stirred water bath.

2.6. X-ray Powder Diffraction. X-ray diffraction (XRD) measurements were performed on a Panalytical Empyrian diffractometer using Cu Kα radiation and PIXCel^{3D} detector in addition to automatic divergence slit, beta filter, and 0.04 rad Soller slits on the incident and diffracted beam side. Variable-temperature measurements were performed using an Anton Paar HTK16N high-temperature strip heater chamber.

2.7. Solid-State P-31 Magic-Angle Spinning Nuclear Magnetic Resonance. The ^{31}P CP MAS NMR spectra were recorded on a Bruker 400 ultrashield VS spectrometer with a 12 kHz MAS spinning rate using Bruker MAS probes (4 mm rotors). The typical contact time was 2−3 ms, and the typical recycle delay was 5−30 s. The ^{31}P MAS NMR data were acquired using a single-pulse (Bloch decay) experiment with and without strong ^{1}H decoupling ($B_{1H} \approx 80$ kHz) during acquisition. The measured ^{31}P chemical shifts were indirectly referenced to the primary ^{31}P reference of 85% H_3PO_4 (δ_{iso} = 0.0 ppm) via a secondary solid reference of ammonium dihydrogen phosphate $(NH_4)H_2PO_4$.

2.8. Thermal Analysis. Thermogravimetric analysis-differential thermal analysis-mass spectrometry (TGA-DTA-MS) analyses were performed with a Setaram Setsys Evolution 16 Instrument under flowing air heated at 5 °C/min, which was coupled to a Hiden QGA300 Instrument for gas analysis. TGA-differential scanning caloriimetry (DSC) analyses were accomplished on a TA Instruments Q600 instrument in flowing air.

2.9. Nitrogen Porosimetry. Measurements of nitrogen adsorption−desorption isotherms were performed on a Micromeritics ASAP 2420 instrument.

2.10. Measurement of Sorption Properties. Adsorption properties were measured using mixed cation solutions in 0.10 M HNO_3. Solution A contained Cs^+, Sr^{2+}, La^{3+}, Ce^{3+}, Pr^{3+}, Nd^{3+}, Gd^{3+}, Dy^{3+}, Ho^{3+}, Co^{2+}, and Th^{4+} at a concentration of ∼0.10 mmol/L (∼20 mg/L) for a total ionic strength of ∼1 mmol/L. Solution B was prepared by a 10-fold dilution of solution A so that the total ionic strength was 0.10 mmol/L and individual cation concentrations were ∼1−2 mg/L.

The distribution coefficient (K_d), which is simply a mass-weighted partition coefficient, was calculated according to the following equation:

$$K_d = \frac{(C_i - C_f)}{C_f} \times \frac{V}{M}$$

Here C_i and C_f are the initial and final concentrations, respectively, M is the mass of adsorbent used in grams, and V is the volume of solution treated in milliliters. Unless otherwise stated the volume-to-mass (mL/g) ratio used for the experiments was set at 120. Kinetics data were treated using the pseudo-second-order rate law as described by Ho et al.[46,47]

$$\frac{dq_t}{dt} = k(q_e - q_t)^2$$

Here q_t is the amount of target ion sorbed in milligrams per gram of adsorbent at time t, q_e is the amount of metal ion sorbed at equilibrium in milligrams per gram of adsorbent, and k is the rate constant (g/mg min).

Quantification of the elements in solution was achieved using a Bruker S2 Picofox total external reflection X-ray fluorescence spectrometer (TXRF). To 990 μL of each solution to be analyzed was added 10 μL of an internal standard (Ga), and then 10 μL of this solution was pipetted onto a quartz analysis plate. Uncertainties relating to the TXRF analyses for the heavy elements concerned were determined by repeated measurement of different samples of the same concentration. These uncertainties were estimated to be of the order of ±5%.

3. RESULTS

3.1. X-ray Powder Diffraction. In Figure 1 are shown the X-ray powder diffraction patterns of a series of ZrBTP-x materials synthesized by combining varying proportions of $ZrOCl_2{\cdot}8H_2O$ and BTP in water such that a precipitate formed spontaneously. The spontaneous formation of a precipitate attests to the very low solubility of the Zr(IV)-BTP compounds. The precipitates were then reacted hydrothermally (160−170 °C). The XRD pattern of the precipitate obtained from composition ZrBTP-0.7 (Figure 1a) showed that it was not totally X-ray amorphous possessing two very broad reflections at 11.5 and 22.4° 2θ. Scherrer analysis indicates that the particle size for these materials was ∼2 nm. XRD patterns of the hydrothermally treated suspensions having different values of x are shown in Figure 1b−e. Compared to the non-hydrothermally treated precipitate, the hydrothermally treated ZrBTP-0.7 phase was clearly more crystalline (Figure 1b). As the mole fraction of phosphorus increased (x) the crystallinity seemed to improve, with the ZrBTP-0.8 phase appearing to be the most crystalline phase possessing a series of broad reflections at 11.5, 20.0, and 22.4, and 28.1° 2θ. These materials are therefore clearly more crystalline than the previously reported Zr-ATMP[40] and Zr-zoledronate[41] coordination polymers that showed no X-ray reflections. Also shown

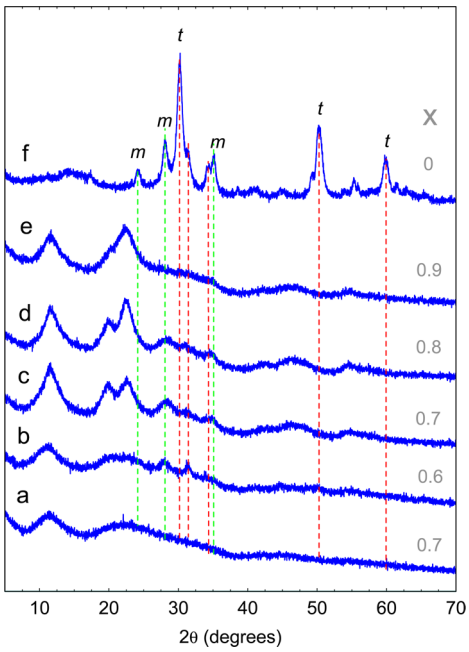

Figure 1. X-ray powder diffraction patterns of Zr(IV)-BTP-x materials (a) ZrBTP-0.7 precipitate, (b−e) ZrBTP-0.6, ZrBTP-0.7, ZrBTP-0.8, and ZrBTP-0.9, (f) ZrO_2 precipitate from $ZrOCl_2{\cdot}8H_2O$.

DOI: 10.1021/acs.inorgchem.6b00954
Inorg. Chem. XXXX, XXX, XXX−XXX

in Figure 1f is the pattern of a precipitate obtained by the direct precipitation of hydrated zirconia through the addition of NaOH solution to a solution of $ZrOCl_2 \cdot 8H_2O$ following by the same hydrothermal treatment. The XRD pattern indicates the formation of monoclinic (m) and tetragonal zirconia (t) of very small particle size. The particle sizes for these phases as determined by Scherrer analysis were between 10 and 15 nm.

Given that the main reflections of the either monoclinic or tetragonal zirconia phases present in the precipitate at 24.1 (m), 28.0 (m) 30.2 (t), 31.3 (m), 34.2 (m), 50.3 (t), and 59.9° (t) 2θ could not be clearly discerned in the pattern of any of the ZrBTP-x phases it would appear that zirconia is not present, at least in significant concentrations. Also arguing against the existence of ZrO_2-like Zr−O−Zr bonding in these compounds is the fact that the bands of ZrO_2 (530, 620, and 725 cm^{-1}) are not evident in the Fourier transform infrared (FTIR) spectra of this series of compounds (Figure S1 of Supporting Information section).[48]

It was observed in additional experiments in which HNO_3 was added to the precipitate prior to hydrothermal treatment that somewhat more crystalline materials could be produced (see Figure S2 of Supporting Information section) by increasing the acidity of the suspension. It was also observed (Figure S3 Supporting Information section) that a change of solvent from water to ethanol and other solvents preserved the essential features of the XRD patterns for all compositions, although increased broadening was observed in some cases.

Cation binding experiments to be described later in this paper indicated that the best-performing materials were the ZrBTP-0.8 and ZrBTP-0.9 phases, and therefore initial efforts focused on optimizing these materials.

With the aim of reducing the possibility of precipitating zirconia and increase crystallinity, a series of syntheses were undertaken in which increasing amounts of HF were added to the ZrBTP-0.8 precursor composition to mineralize any zirconium oxyhydroxide that might form under the hydrothermal conditions thus maintaining Zr(IV) in solution. The XRD patterns of these materials are shown in Figure 2. It can be observed that as the F/Zr molar ratio in the hydrothermal preparations was increased the products became increasingly crystalline. Presumably this is a result of the mineralization of oxyhyroxide zirconium species in solution. What is apparent from this series of XRD patterns is that regardless of the amount of HF used, the phase or phases being generated were always similar differing only in the degree of order. This would seem to include even the precipitate that was directly generated by addition of BTP to $ZrOCl_2$ solution (Figure 1a).

For the remainder of this paper, and as a matter of convenience, materials prepared without the use of HF and giving XRD patterns such as in Figure 2a are referred to as Gen I, those prepared with the use of small amounts of HF and giving XRD patterns such as those of Figure 2b,c are referred to as Gen II, and those giving XRD patterns of crystalline materials such as in Figure 2d,e as Gen III.

It is also very important to note that in none of these patterns could ZrO_2 phases be identified. In fact, close inspection of the XRD patterns of Figure 2b−e suggests the presence of at least two phases characterized by both relatively broad (indicated by ↓) and sharp reflections.

Attempts to index the series of sharp reflections were not successful mainly because a unique unit cell could not be encountered. In part this could be because it is likely that all reflections are not due to a single phase.

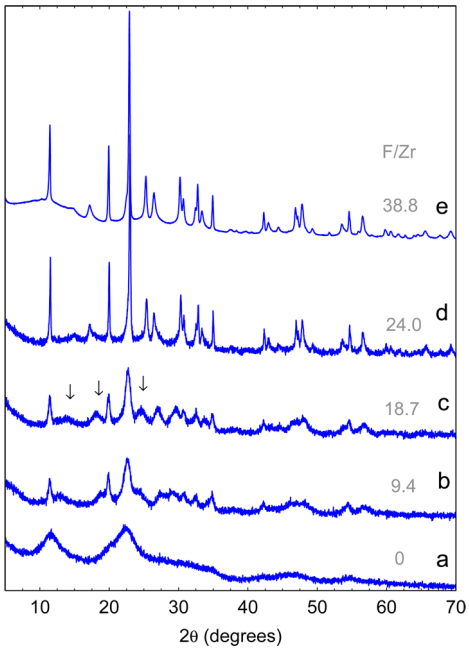

Figure 2. X-ray powder diffraction patterns of materials synthesized as a function of the F/Zr molar ratio. (a) ZrBTP-0.8−0, (b) ZrBTP-0.8−9.4, (c) ZrBTP-0.8−18.7, (d) ZrBTP-0.8−24.0, (e) ZrBTP-0.8−38.8.

Scherrer analysis of the sharpest patterns indicated a particle size in the range of 100−300 nm for all phases. This was more than an order of magnitude larger than was obtained for the materials prepared in the absence of mineralizing agent.

3.2. Nitrogen Porosimetry. The adsorption−desorption isotherms for the series of the Gen I ZrBTP-x samples prepared without the use of HF and having the diffraction patterns of Figure 1 are shown in Figure 3a. For this series of samples all isotherms were essentially type II that are indicative of nonporous or macroporous materials with wide pore-size distributions. The Zr-BTP-0.7 phase had the highest BET surface area (500 m^2/g) and Zr-BTP-0.6 and ZrBTP-0.8 present similar surface area (279 and 247 m^2/g, respectively). The ZrBTP-0 sample, or in other words the ZrO_2 precipitate, had a relatively low BET surface area (80 m^2/g). As the value of P/(Zr + P) increased so too did the extraction capacity of the material (see later).

The adsorption−desorption isotherms for the series of ZrBTP-0.8-f samples synthesized using increasing amounts of HF corresponding to the diffraction patterns of Figure 2 are shown in Figure 3b. It is apparent that for ZrBTP-0.8−0, ZrBTP-0.8−24, and ZrBTP-0.8−38.8 the isotherms are clearly of Type II, while for ZrBTP-0.8−9.4 and ZrBTP-0.8−18.7 the isotherms are distinctly of Type IV with a type H2 hysteresis loop. The surface areas measured by nitrogen porosimetry follow a similar pattern as a function of HF content as determined by small-angle X-ray scattering measurements (see Figure S4 of Supporting Information section).

From Figure 4b it can be observed that as the amount of fluoride included in the synthesis increased, the samples became more crystalline, and the surface areas decreased. Type IV isotherms were observed for Zr-BTP0.8−9.4 and Zr-BTP0.8−18.7 and signal that a significant change in porous texture occurred in these samples (Figure 3b).

For the ZrBTP-0.8-f compositions, increasing Zr/F and therefore crystallinity trends with decreasing surface area as

DOI: 10.1021/acs.inorgchem.6b00954
Inorg. Chem. XXXX, XXX, XXX−XXX

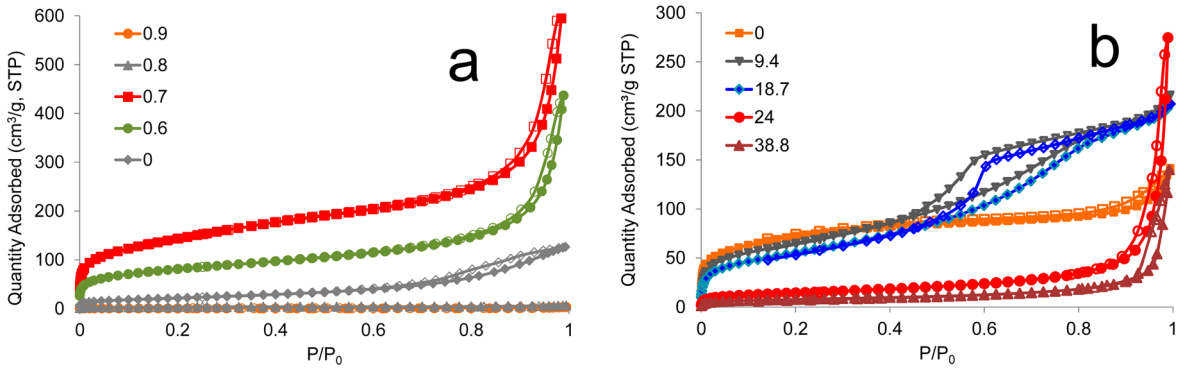

Figure 3. Nitrogen adsorption−desorption isotherms of (a) ZrBTP-x samples with variable *x* and prepared without HF and (b) ZrBTP-0.8-HF using increasing amounts of HF in the range from 0 to 39. Closed symbols correspond to the adsorption branch; open symbols indicate the desorption branch.

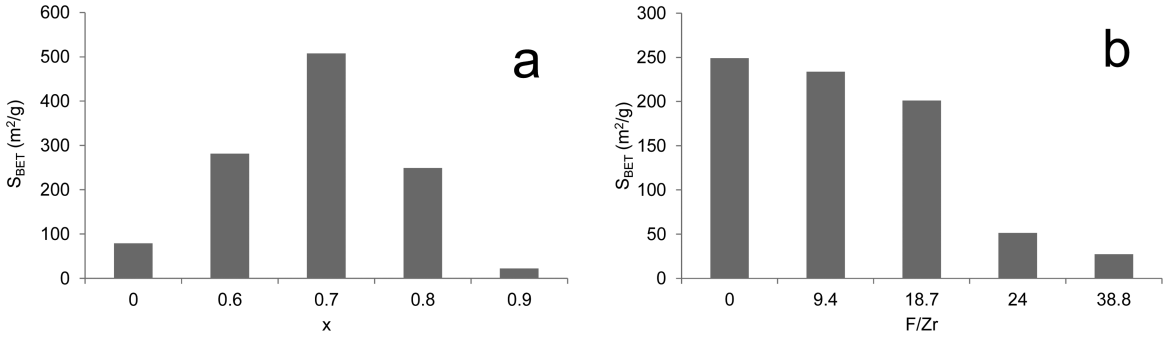

Figure 4. BET surface areas of (a) ZrBTP-x series prepared without HF and (b) ZrBTP-0.8-HF using increasing amounts of HF.

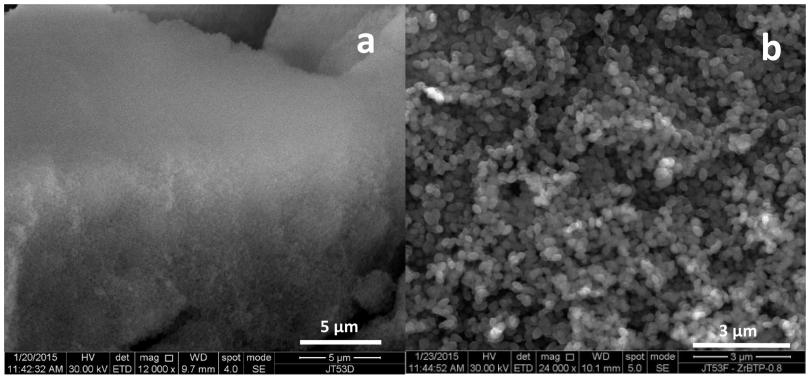

Figure 5. Backscattering electron images of crystalline ZrBTP-0.8−24 at low (a) and high (b) magnification.

expected. This in turn resulted in reduced adsorption capacity for cation extraction as also expected.

3.3. Scanning Electron Microscopy. Scanning electron microscopy could not be used to observe images of the particles of the less crystalline Gen I samples ZrBTP-0.8−0, ZrBTP-0.8−9.4 and ZrBTP-0.8−18.7 due to the small grain size. In this case TEM was found to be more appropriate.

For the more crystalline samples such as ZrBTP-0.8−24 having well-defined diffraction patterns and Type II nitrogen adsorption isotherms, discrete roughly spherical particles with diameters of the order of 50 nm were observed (Figure 5). Particles of this dimension should give surface areas of 30 m^2/g assuming a density of ~4 cm^3/g. This value of area is close to what is actually measured. Such particle diameters were also roughly in line with what was measured by the Scherrer analysis. In other words, to first approximation, the surface area of these materials is due to external particle surfaces.

For more crystalline samples of ZrBTP-0.8 prepared using HF (Figure 2e) Scherrer analysis yielded particle diameters in the 20−50 and 150−200 nm ranges. This appears consistent with what was observed in SEM images where spherical particles can be observed at high magnification (Figure 5b). For less crystalline samples clear particle morphologies could not be observed using SEM.

In some cases elongated nanoparticles of approximately the same dimensions were observed. This particle size was entirely consistent with the aforementioned Scherrer analysis. At the length scale being probed no other morphologies were evident suggesting that the sample could be monophasic. The average of numerous EDAX analyses over wide and narrow areas of the sample gave an average phosphorus mole ratio (P/(Zr + P)) of 0.82 for the ZrBTP-0.8 sample of Figure 1a. This value is very close to the value expected based on initial reactant mole ratios confirming that all the phosphorus that was included in the

DOI: 10.1021/acs.inorgchem.6b00954
Inorg. Chem. XXXX, XXX, XXX−XXX

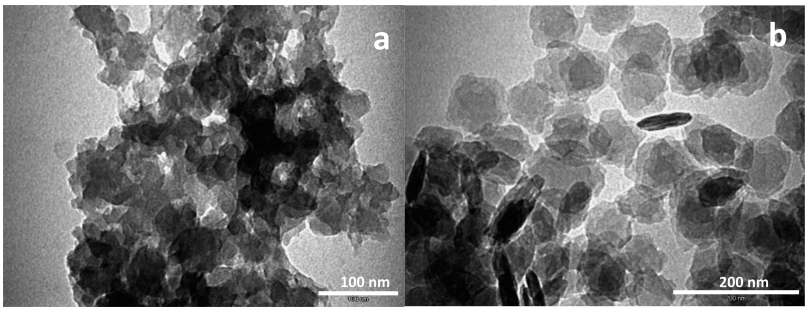

Figure 6. TEM images of ZrBTP-0.8 (a) GEN I and (b) GEN III (ZrBTP-0.8−23.8).

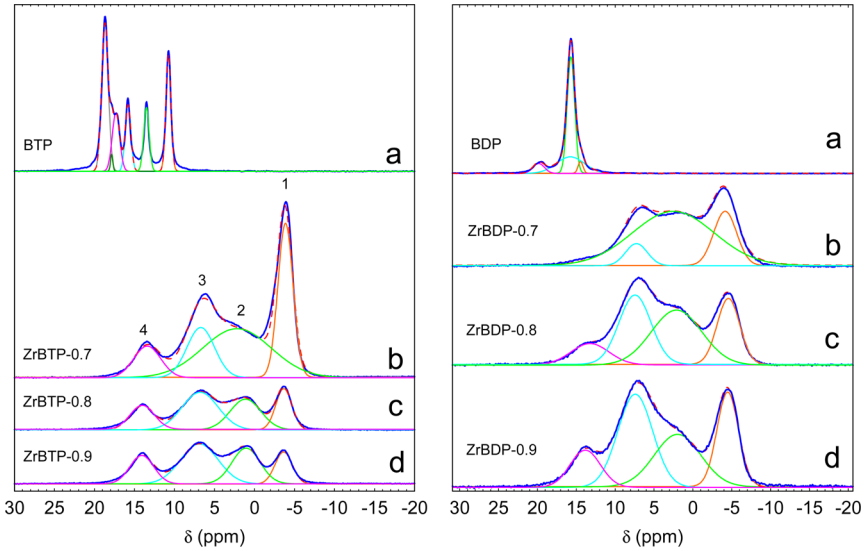

Figure 7. ^{31}P MAS NMR of ZrBTP-x and ZrBDP-x samples. The different resonances are labeled 1−4 for convenience.

precursor solution was incorporated into the final product. This was also the case for sample of Figure 1b.

3.4. Transmission Electron Microscopy Imaging. Figure 6 shows the TEM images of Gen I and III materials. For the Gen I materials prepared in the absence of HF (Figure 6a) the grain size was very fine and only just observable. It is estimated that the particles were of the order of 10 nm in diameter. Such particles would be expected to yield surface areas of at least 150 m^2/g, which were observed ($247 m^2/g$ for Zr-BTP-0.8−0).

For the Gen III materials, two particle morphologies were observed in the TEM images including round particles and elongated particles (Figure 6b). These particles appeared to have relatively narrow size distributions. Analysis of the occasional round particle that could be found isolated from the other particles showed them to be quite crystalline.

3.5. Solid-State Phosphorus-31 Magic-Angle Spinning Nuclear Magnetic Resonance. Phosphorus-31 is an S = 1/2 nucleus, has a high isotopic abundance, high sensitivity, and shows a large chemical shift range. Despite the fact that phosphorus is an important element in many biomaterials and that it is increasingly important in the context of the design and preparation of open framework materials, there exists a surprising paucity of systematic solid-state ^{31}P NMR work on phosphonate compounds.

Single-pulse solid-state ^{31}P MAS NMR spectra were recorded of the different ZrBTP-x and ZrBDP-x samples along with the free acids (Figure 7). These spectra are superficially similar to those published by Brunet et al.[49] for microporous materials formed from aluminum and 4,4-biphenyldiphosphonic (BPDP). These aromatic polyphosphonates bear some similarities to the BTP except that the phosphonate groups are on adjacent carbons rather than alternate carbons as in BTP. In the work by Brunet et al., no specific assignments were made in the ^{31}P MAS NMR, which like the present materials also contained four or more resonances.

The MAS NMR spectrum of solid BTP acid shows a group of six relatively sharp resonances having isotropic shifts ranging from 18.7 to 10.7 ppm (Figure 7a). The spectrum is indicative of six chemically distinct P sites that are likely distinguished in terms of the degree of protonation.

When the phosphonate ligands complex Zr(IV) as in the precipitation of ZrBTP-0.7 to ZrBTP-0.9 and ZrBDP-0.7 to ZrBDP-0.9 (Figure 7) four discrete broad isotropic shifts (1−4) are observed. These four resonances are shifted significantly upfield from that of the free acids. The chemical shifts span a range from −4 ppm for resonance one to 14 ppm for resonance four. There was no dependence of the spectra on the nature of the solvent used for the syntheses. The reduction in the number of resonances, the broadening, and the upfield shifts are indicative of significant changes in the phosphonate bonding as might be expected on complexation with Zr(IV). Similar general trends, including the chemical shift spread, are consistent with what was observed in the Zr-zoledronate[41] and Zr-ATMP[40] coordination polymers reported recently. The increased broadening of the spectra of the ZrBTP-x samples

DOI: 10.1021/acs.inorgchem.6b00954
Inorg. Chem. XXXX, XXX, XXX−XXX

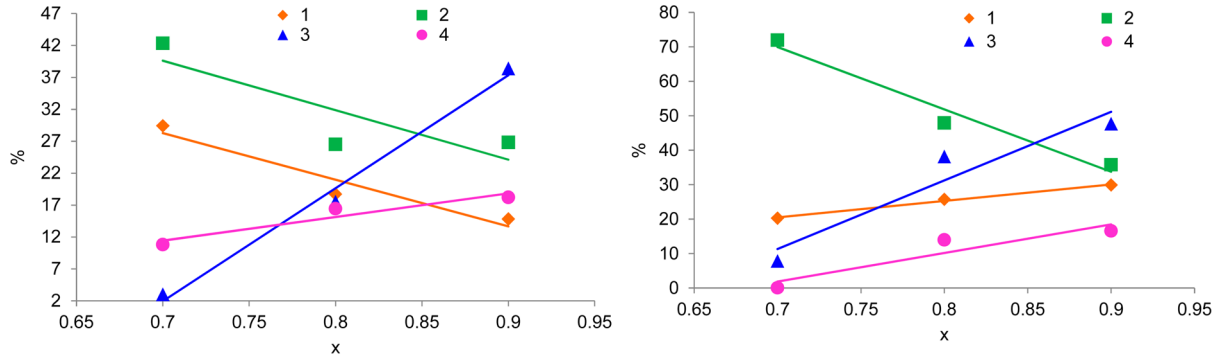

Figure 8. Intensities of the various ^{31}P resonances as a function of phosphorus content for ZrBTP-x (left) and ZrBDP-x (right). The lines are only intended to serve as a guide.

relative to BTP itself is consistent with a loss of order. The spectra of the Zr-benzene phosphonates, however, differ in two important respects relative to the other mentioned systems. First the difference between the center of mass of the spectra of the free acids and the Zr-zoledronate and Zr-ATMP polymers was minimal, whereas the center of mass of the Zr-benzene phosphonates was shifted significantly upfield relative to the free acids. Second, in the Zr-zoledronate and Zr-ATMP systems new upfield resonances were observed, as the phosphorus content increased, that were attributed to the generation of relatively uncondensed and deprotonated phosphonate groups. These additional upfield shifts were assigned in a manner consistent with available information on ^{31}P MAS NMR, especially the work of Josse et al.[50]

The striking difference between the ^{31}P MAS NMR of the ZrBTP-x and Zr-zoledronate system is that in the ZrBTP-x system there is generally little or no change in either the number or the frequency of the four isotropic shifts observed as the mole ratio of phosphorus is increased. What changes as a function of phosphorus content is the relative intensities of the various resonances.

The ^{31}P MAS NMR spectra of the ZrBDP-x (and also the ZrBMP-x see Figure S5 of Supporting Information section) materials are remarkably similar to those of the ZrBTP-x samples in that they contain four resonances at similar frequencies with all being displaced upfield relative to the BDP by approximately the same amount. Although the spectra of all the ZrBDP-x samples contain four resonances for the ZrBDP-0.7 sample resonance 4 is barely discernible and was not fitted. As in the case of the ZrBTP-x system the relative intensities of the resonances varies as a function of phosphorus content. Spectral fitting facilitated the measurement of the relative intensities of these resonances that are plotted in Figure 8.

The plots of Figure 8 show that the variation in relative intensities of resonances 2−4 as a function of phosphorus content is similar for both BTP- and BDP-derived materials, all increasing with phosphorus content. However, resonance one decreases for ZrBTP, whereas it increases for ZrBDP as a function of *x*. It would however be imprudent to place too great a significance on this relatively minor difference between the three systems. In fact what seems remarkable is the similarity of the different systems and the invariance in the trends in intensities of the various resonances as a function of *x*. It is suspected that this has to do with the rigidity of the ligands and the distance between phosphonate and carboxylate groups. To advance beyond this interpretation would require the use of advanced multipulse sequences that can provide information on the phosphonate connectivity.[51]

3.6. Thermal Analysis. The samples prepared in this study were subjected to thermal analysis primarily to assess their stability. The TGA-DTA of the ZrBTP-0.8-H_2O as a representative of the family of ZrBTP-0.8 prepared in water solvent is shown in Figure 9a. The weight loss that commences at ∼50 °C and ends at ∼150 °C was due to the loss of adsorbed water as shown by the real-time mass spectrum recorded of the products released at the reactor outflow during the heating ramp. Following the loss of the weakly bound water a gradual weight loss then occurs between ∼455 and 608 °C. Thereafter a steep weight loss occurs that is due to decomposition of the BTP with the only decomposition product being CO_2. No phosphorus was observed at this point in the mass spectrum.

In contrast to the ZrBTP-x phases, the ZrBDP-x phases displayed a more progressive weight loss over the temperature range from 450 to 850 °C, at which point a steep loss was observed (Figure 9c). The mass spectral measurements demonstrated that the gradual weight loss was due to the breakdown of organic groups with emission of CO and CO_2. Once again, no phosphorus was detected at any temperature suggesting that all phosphorus is retained in the product until at least 1200 °C. The fact that CO is generated in addition to CO_2 may be because carboxylate groups are being broken down in addition to the aromatic ring, which seems to only produce CO_2.

Gomez-Alcantara et al.[52] reported the preparation of lamellar microporous aluminum phosphonates from 4-(4-phosphonophenoxy)phenyl phosphonic acid (PPPA) and observed decomposition at temperatures between 400 and 600 °C. The difference in total weight loss between ZrBTP-0.8 and ZrBDP-0.8 with similar phosphorus mole fraction (P/(Zr + P) is really due to the increasing organic content of the latter sample for a given total mass.

3.7. In Situ Variable-Temperature X-ray Diffraction. In situ variable-temperature XRD was undertaken in air of ZrBTP-0.8 in an attempt to shed light on the mechanism of its thermal decomposition (Figure 10) and to differentiate possible phases in terms of their thermal stabilities.

The pattern at 200 °C is identical to that recorded at 25 °C and remains relatively unchanged until at least 500 °C. What is striking about this series of patterns is the disappearance at 700 °C of the reflections marked by the heart-shaped symbol that were observed in the range of 25−600 °C to leave a reduced set of sharp reflections marked by ♦. This series of sharp reflections could be well-indexed on a face-centered cubic

DOI: 10.1021/acs.inorgchem.6b00954
Inorg. Chem. XXXX, XXX, XXX−XXX

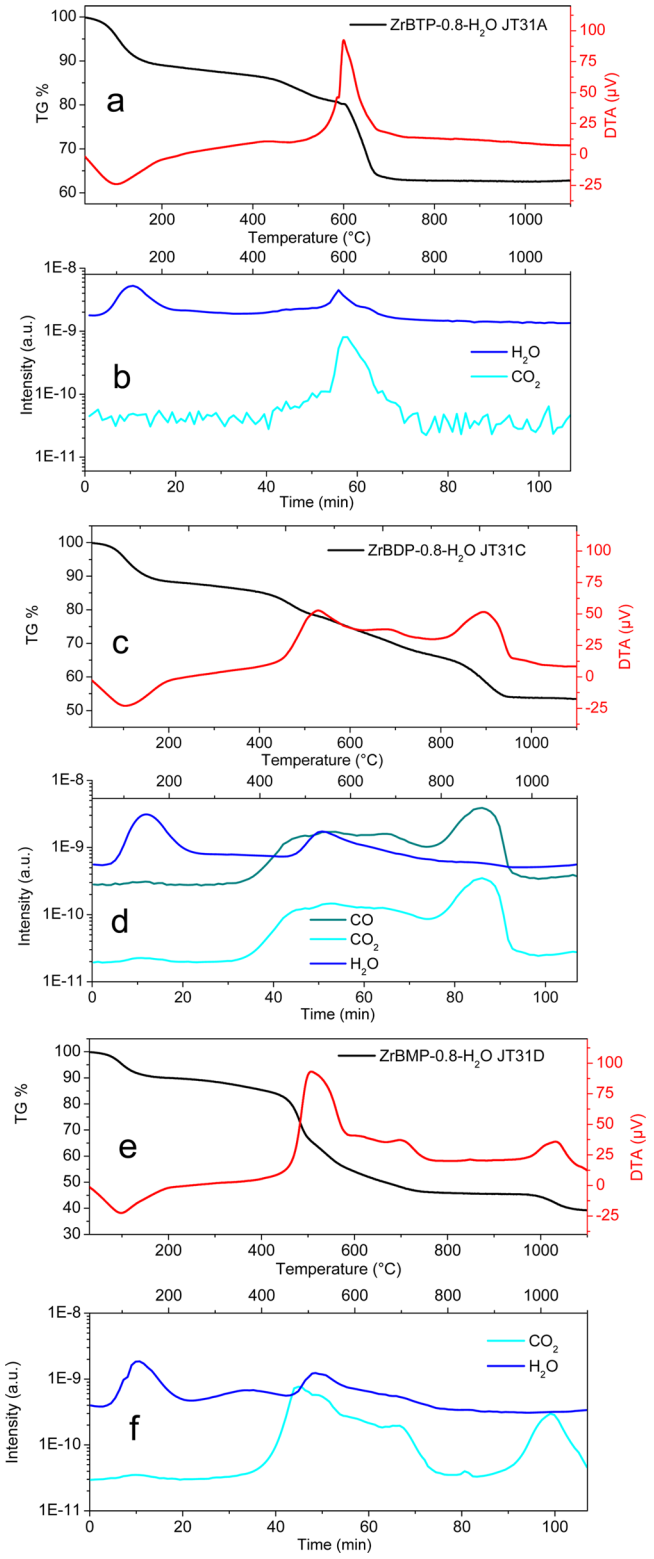

Figure 9. Thermal analysis in air and mass spectra, respectively, of (a, b) ZrBTP-0.8, (c, d) ZrBDP-0.8, (e, f) ZrBMP-0.8.

cell. By deduction it appears that the patterns indicated by both the heart-shaped symbol and ♦ are from discrete relatively crystalline phases. In other words, the synthesized ZrBTP-x materials contain at least two relatively crystalline phases. Also present in the low-temperature patterns are a series of broader reflections that could be from a third phase.

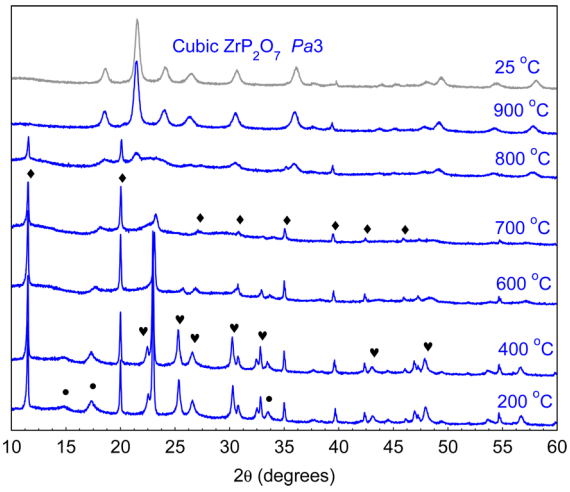

Figure 10. In situ variable-temperature X-ray powder diffraction patterns of ZrBTP-0.8.

As the temperature was increased beyond 800 °C a phase transition occurred with coalescence of all phases into a single cubic ($Pa\bar{3}$) pyrophosphate structure (ZrP_2O_7). In fact the pattern at 900 °C appears relatively uncontaminated, and successful Rietveld analysis could be undertaken giving a unit cell parameter of 8.2849 Å (see Figure S6 of Supporting Information section).

3.8. Cation Binding. Screening of the poorly crystalline Gen I ZrBTP-x extractants with different mole ratios of phosphorus was initially performed using the high ionic strength mixed cation solution (1 mmol/L) with nominal concentration of individual cations of 20 mg/L in 0.1 M HNO_3 (solution A), and the data are shown in Figure 11. The use of

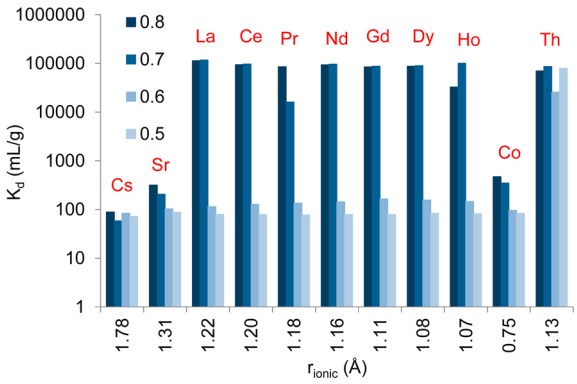

Figure 11. Extraction of cations of different ionic radius by poorly crystalline ZrBTP-0.8, ZrBTP-0.7, ZrBTP-0.6, ZrBTP-0.5, prepared in the absence of HF from mixed cation solutions with each cation at nominal 20 mg/L in 0.10 M HNO_3 (Solution A). The V/M ratio was 100.

mixed cation solutions was justified on the basis that applications of the materials at the back-end of the present or future nuclear fuel cycles or rare-earth mineral processing will always encounter mixtures of all LNs. The data are ordered according to decreasing ionic radii except for the case of Th^{4+} (r = 1.13 Å), which is placed at the end of the horizontal axis for clarity. The data show that, for ZrBTP-0.8 and ZrBTP-0.7, the order of increasing selectivity is $Cs^+ < Sr^{2+} = Co^{2+} < LN^{3+} < Th^{4+}$ or in other words the selectivity depends to first order on cation valence and cation polarizability as in a typical

DOI: 10.1021/acs.inorgchem.6b00954
Inorg. Chem. XXXX, XXX, XXX−XXX

Hofmeister series.[53] As the mole fraction of phosphorus in the adsorbents decreased (ZrBTP-0.6 and ZrBTP-0.5) so too did the overall K_d values. This suggests that the cation binding capacity in these materials is driven principally by the availability of phosphonate groups. To test this hypothesis it is expected that the FTIR of lanthanide- and thorium-loaded extractants would show shifts in the vibrational spectrum of the phosphonate groups as was observed for the Zr(IV)-zoledronate system.[41]

Experiments were conducted to ascertain the extraction efficiency of Zr(IV)-polyphosphonates prepared from the different polyphosphonate ligands in the absence of HF (Gen I materials). In Figure 12a are shown the distribution

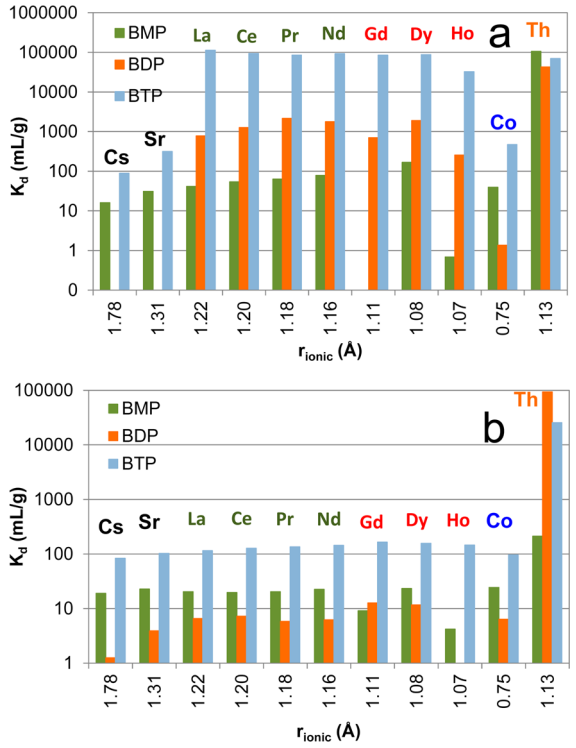

Figure 12. Extraction of cations of different ionic radius by GEN I (a) ZrBTP-8, ZrBDP-0.8, and ZrBMP-0.8 (b) ZrBTP-0.6, ZrBDP-0.6, and ZrBMP-0.6 from mixed cation solutions with each cation at nominal 20 mg/L in 0.10 M HNO_3 (solution A). Elements are ordered according to decreasing ionic radii except for Th.

coefficients measured for ZrBTP-0.8, ZrBDP-0.8, and ZrBMP-0.8 prepared in the absence of HF. In general the extraction efficiency (K_d) measured using solution A was reduced as the number of phosphonic acid groups per benzene unit was reduced. Because these experiments were conducted with mixed cation solutions having relatively high ion strength with nominal individual cation concentrations of 20 mg/L and at fixed volume-to-mass ratio, the reduction in K_d could reflect the reduced capacity of the material as the contribution of organic to the total mass of each sample increased. Put another way, although ZrBTP-0.8, ZrBDP-0.8, and ZrBMP-0.8 all have the same overall phosphorus molar ratio (P/(Zr + P)) this series of compounds has decreasing numbers of phosphonic acid groups per unit mass, and therefore reduced capacity is not unexpected. That the overall dependence of K_d values on ionic radii was relatively constant irrespective of the substitution of carboxylate groups for phosphorus suggests that the behavior of the materials is essentially determined by the phosphonate binding groups.

For low ion strength solutions (total cation concentration of ~0.1 mmol/L) in which individual cation concentrations were between 1 and 2 mg/L (Figure 13), the dependence of K_d on

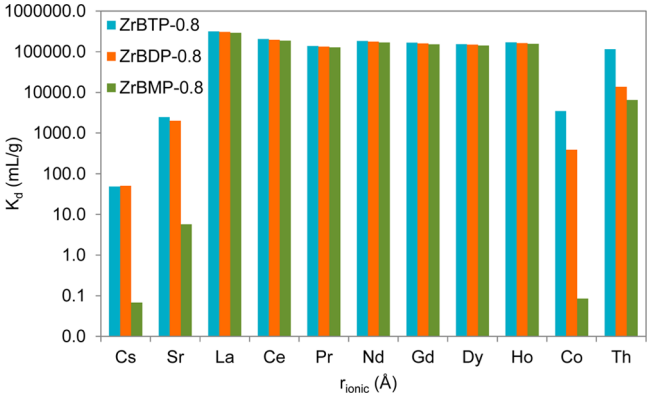

Figure 13. Extraction of cations of different ionic radius by Gen I ZrBTP-0.8, ZrBDP-0.8, and ZrBMP-0.8 from low ionic strength mixed cation solutions with each cation at nominal 2 mg/L in 0.10 M HNO_3 (solution B). Elements are ordered according to decreasing ionic radii except for Th.

cation radius for Gen I materials was similar as obtained using the higher ion strength solutions. That is, strong sorption of trivalent lanthanides with much weaker sorption of monovalent (Cs^+) and divalent cations (Sr^{2+} and Co^{2+}) obtained.

Unlike the situation of extraction from the high ionic strength solutions (solution A), extraction of all lanthanides from the low ion strength solution (solution B) was quantitative for ZrBTP-0.8, ZrBDP-0.8, and ZrBMP-0.8. This difference in lanthanide extraction on total cation concentration is therefore likely to be due to the reduced availability of free phosphonic acid groups in the latter material despite the fact that the overall phosphorus mole fraction was constant.

To evaluate the extraction efficiency of the Gen II (ZrBTP-0.8−9.4, ZrBTP-0.8−24) and Gen III (ZrBTP-0.8−38) materials shown in the XRD patterns of Figure 2, batch contact experiments were conducted using the low ion strength solutions. The data of Figure 14 show that all materials extracted lanthanides more or less quantitatively across the series. Another striking feature of these data is that for these Gen II and III materials there is virtually no adsorption of Cs^+ and very little adsorption of Sr^{2+}.

It is well-appreciated that at very low ionic strengths, K_d is close to being a true equilibrium concentration between cations in solution and binding sites on the adsorbent surface. In this study the lower concentration limit was essentially set by the detection limit of the measurement technique (TXRF). As concentration is increased additional equilibria come into play between lanthanides and availability of the different surface binding sites with possibly different binding energies. This is manifest by the dependence of K_d on total cation concentration in solution of the survey measurements.

In an attempt to determine the total capacity of the most effective Gen I ZrBTP-0.8 materials we first measured the Ce(III) adsorption isotherm (Figure 15) in 0.10 M HNO_3. The isotherm was of L-type,[54] and adsorption did not reach a plateau even up to the highest equilibrium cation concentrations used. The isotherm is fitted relatively well by Toth,

DOI: 10.1021/acs.inorgchem.6b00954
Inorg. Chem. XXXX, XXX, XXX−XXX

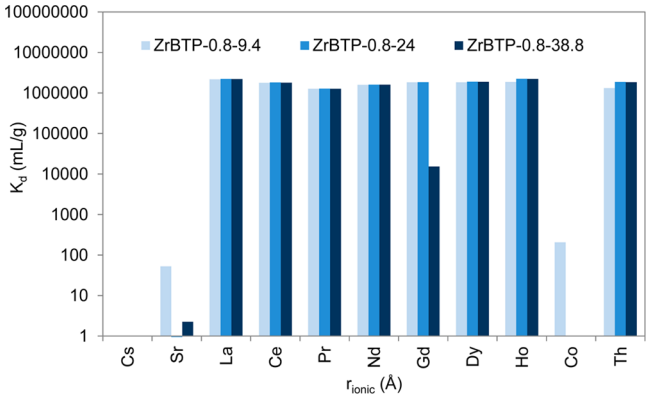

Figure 14. Distribution coefficients for cations of different ionic radius by Gen II (ZrBTP-0.8−9.4, ZrBTP-0.8−24) and Gen III crystalline Zr(IV) organophosphonates (ZrBTP-0.8−38 from), and mixed cation solutions with each cation at nominal 2 mg/L in 0.10 M HNO_3 (solution B). Elements are ordered according to decreasing ionic radius except for Th.

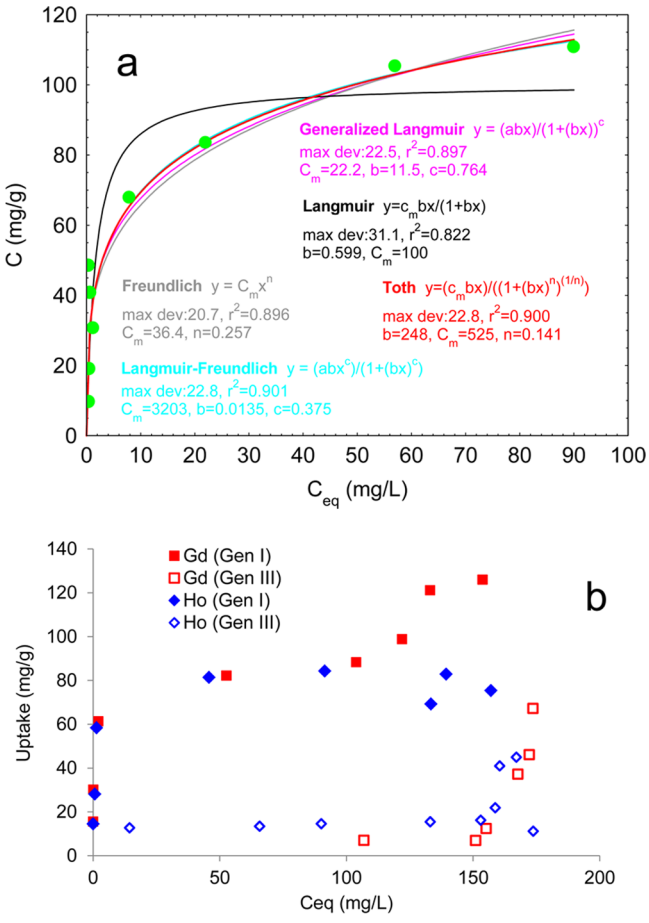

Figure 15. Adsorption isotherm in 0.10 M HNO_3 for (a) Ce^{3+} on poorly crystalline Gen I ZrBTP-0.8 material and (b) Gd^{3+} and Ho^{3+} on Gen I and Gen III materials.

Langmuir, and Freundlich models. The value taken as the capacity of this material for Ce(III) depends on the model that is considered best. Clearly in the given situation the decision is somewhat arbitrary, although it appears that the capacity is somewhere greater than 100 mg/g.

To compare the performance of the poorly crystalline Gen I and crystalline Gen III materials, adsorption isotherms were measured for Gd^{3+} and Ho^{3+} as individual cations under similar experimental conditions (25 °C and 0.10 M HNO_3). For the Gen I ZrBTP-0.8 material, both isotherms show a similar appearance at low equilibrium cation concentrations (Figure 15b). However, unlike the case of Ce^{3+} adsorption on Gen I materials, a definite plateau is reached at ∼100 mg/g adsorbent for these materials at equilibrium cation concentrations between 50 and 100 mg/L for both Gd^{3+} and Ho^{3+}. The data for the Gd^{3+} shows in addition a tendency for a second upswing greater than 100 mg/L suggesting perhaps that a contribution from a second phase comes into play at higher cation concentrations. In the case of the Gen III materials a marked reduction in uptake is observed up to equilibrium cation concentrations of 150 mg/L followed by what appears to be an upswing.

Because the applications being considered here will ultimately involve complex acidic mixtures of cations, and recognizing that the selectivity is evaluated through measurement of the pseudoequilibrium constant K_d and that this is a function of the equilibrium concentration/ionic strength among other things, we undertook to measure adsorption isotherms of the individual cations from the complex mixtures (Figure 16).

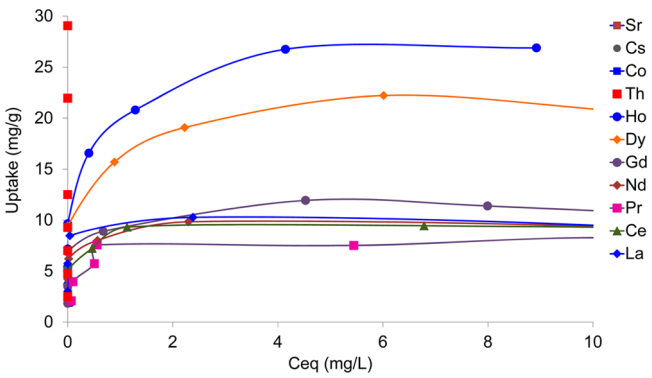

Figure 16. Multiequilibrium adsorption isotherms for ZrBTP-0.8 for mixed cation solutions with each cation at nominal concentration 20 mg/L in 0.10 M HNO_3.

At low equilibrium concentrations strong uptake is observed from most cations in accordance with previously described measurements of capacity. However, as the equilibrium concentration for each cation is increased above ∼1 mg/L it is observed that Dy^{3+} and Ho^{3+} are particularly strongly extracted compared to the other lanthanides. In fact, thorium is quantitatively extracted at all equilibrium concentrations being considered. What these data show is that since the capacity for Th^{4+}, Dy^{3+}, and Ho^{3+} is significantly higher than for the other species the adsorbent would be progressively enriched in these elements. This paves the way for the efficient extraction of these elements from complex solutions. It should be remarked that Cs^{+}, Sr^{2+}, and Co^{2+} were all very poorly extracted at all equilibrium concentrations.

The extraction efficiency of both the ZrBTP-0.8 and ZrBTP-0.8 granulated with PAN in 4 M HNO_3 was measured in solutions of increasing HNO_3 concentrations. The data obtained in 4 M HNO_3 solutions are shown in Figure 17a. Even in concentrated nitric acid solution the present materials are capable of significant extraction of lanthanides with respect to Co^{2+}, which is only very weakly extracted. Moreover, within experimental uncertainty there is a smooth increase in

DOI: 10.1021/acs.inorgchem.6b00954
Inorg. Chem. XXXX, XXX, XXX−XXX

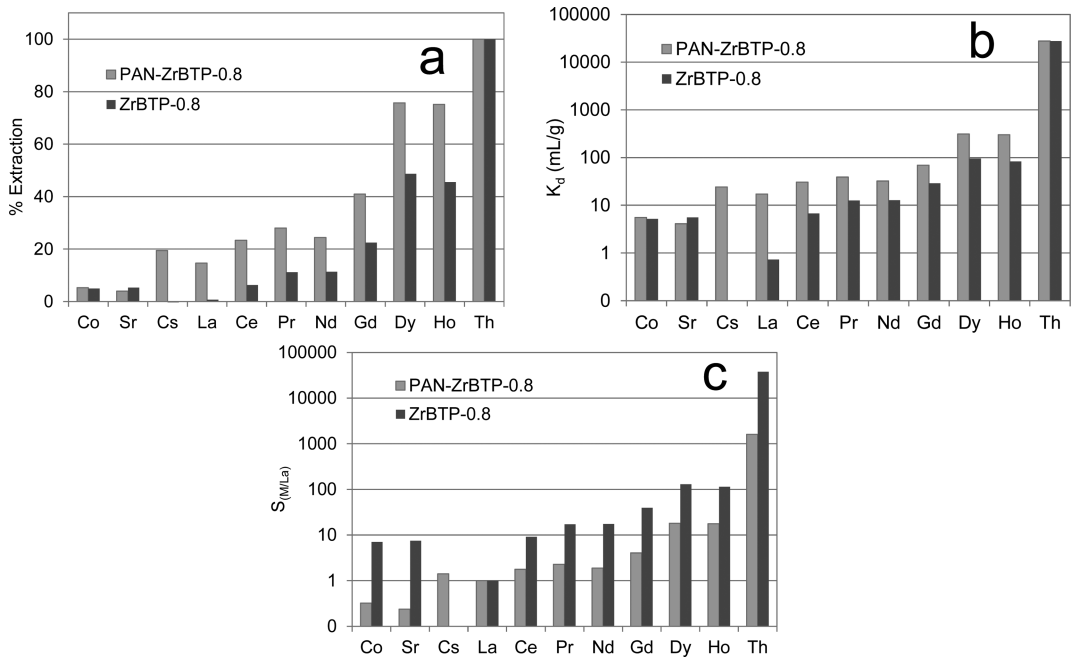

Figure 17. Extraction parameters for ZrBTP-0.8 and granulated PAN-ZrBTP-0.8 measured in 4 M HNO_3 and low ionic strength solutions (0.2 mM) displayed in terms of (a) percentage extraction, (b) K_d, and (c) separation factor.

extraction efficiency as a function of lanthanide atomic number. For a solid extractant the ratio of the K_d values can be considered the distribution ratio or separation factor S. The data of Figure 17c shows that there is a steady increase in S from ~1 to 10 as a function of increasing lanthanide atomic number. Under the given conditions therefore the separation factor between heavy and light lanthanides is easily sufficient for a plausible light-heavy lanthanide separation and probably also an efficient intralanthanide separation.

The separation factor between Th^{4+} and the trivalent LNs is particularly large suggesting that Th^{4+} could easily be separated from a very complex mixture. The PAN-granulated ZrBTP-0.8 system would therefore seem to offer intralanthanide separation comparable to those achievable using alkaline diphosphonic acid extractants only with the associated advantages of solid-phase extractant.[55]

3.9. Thermal Transformation of Cation-Loaded Adsorbents. To address the possibility of disposition of the radiolanthanide and/or actinide-loaded zirconium phosphonates, a range of the Gen I and II materials were saturated with Th^{4+} and Ce^{3+}. Samples were also prepared by saturation with mixtures of lanthanides, and these were then heated to different temperatures both statically and dynamically in the heating chamber of the diffractometer.

Rietveld analysis of a sample of the poorly ordered Th-saturated ZrBTP-0.8 (Gen I) heated directly to 1200 °C in air is shown in Figure 18. Multiple SEM-EDX measurements gave the stoichiometry of the heated sample as approximately $Th_{0.23}Zr_{0.77}P_{1.79}O_{6.5}$. The diffraction pattern could be identified as that of the ZrP_2O_7 pyrophosphate and could be refined on a cubic cell $Pa\bar{3}$ with an a-parameter of 8.3250 Å. During the refinement Th was allowed to occupy the Zr site according to the determined stoichiometry. During refinement this occupancy changed only a little from the initial value. The determined a-parameter was somewhat larger than that obtained for the ZrP_2O_7 without Th included, which gave a value of 8.2849 Å.

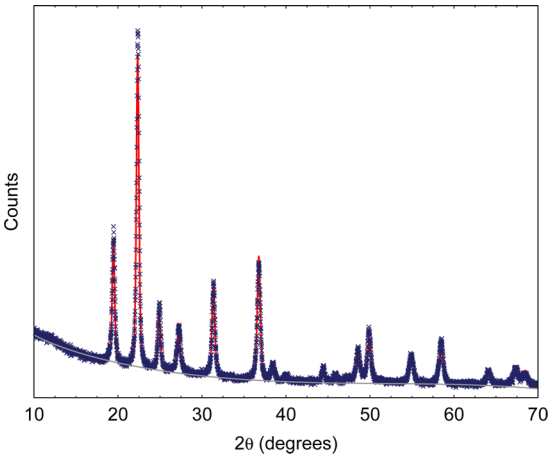

Figure 18. Rietveld analysis of ex situ X-ray powder diffraction pattern of Th-saturated ZrBTP-0.8 heated directly to 1200 °C in air.

In separate experiments, the poorly ordered Gen I ZrBTP-0.8 and Th-loaded ZrBTP-0.8 samples were heated in situ on the high-temperature stage of an X-ray diffractometer. Typically, data were taken every 100 °C with each temperature being attained using a 10 °C/min ramp. The data (Figure 19) show that the pyrophosphate forms abruptly from poorly ordered material at between 700 and 800 °C without any intermediate phase implying a first-order transition.

The variation in unit cell volume as a function of temperature is shown in Figure 20 and shows that, whereas the unit cell volume for the Th-saturated materials undergoes a nonlinear thermal expansion, the cell volume of the as-prepared material remained relatively constant.

Additional experiments with Ce-saturated ZrBTP-0.8 (Gen I) also yielded the pyrophosphate structure with composition $Ce_{0.14}Zr_{0.86}P_{1.76}O_{6.33}$ having unit cell volumes similarly enlarged with respect to the as-prepared ZrBTP-0.8 materials as was the case for the Th-saturated ZrBTP-0.8 materials. Such enlarged

DOI: 10.1021/acs.inorgchem.6b00954
Inorg. Chem. XXXX, XXX, XXX−XXX

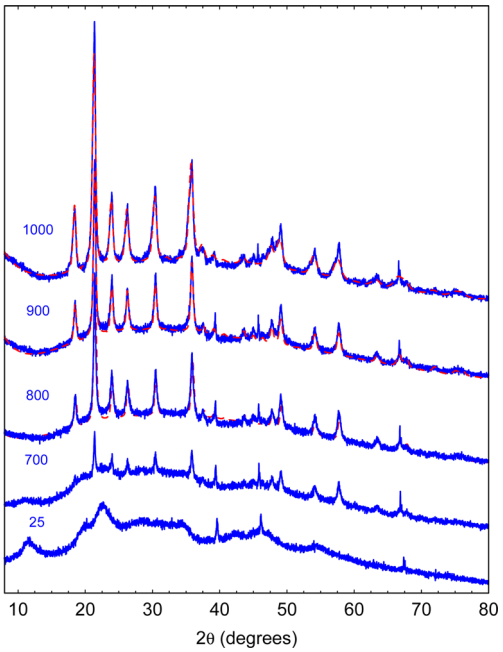

Figure 19. Selected in situ X-ray diffraction patterns at different temperatures of Th-saturated ZrBTP-0.8 and corresponding Rietveld refinements where appropriate.

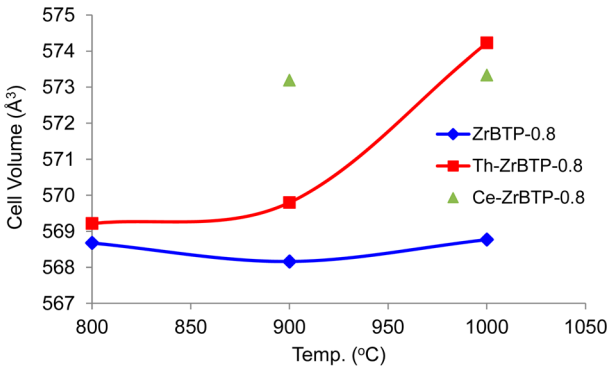

Figure 20. Unit cell volume determined from the Rietveld refinement for Gen I ZrBTP-0.8 material heated to different temperatures before and after being saturated with thorium.

unit cell volumes are consistent with replacement of the smaller Zr^{4+} by the larger trivalent lanthanide and Th^{4+} when in the same coordination.

When the Gen I ZrBTP-0.8 phase was saturated with the range of cations used in the adsorption experiments the only phase produced was the pyrophosphate (see Figure S10 of Supporting Information). Thus, it would appear that the pyrophosphate structure is always favored at least for ZrBTP-0.8 composition (80 mol % P). This might not necessarily be the case for other compositions. Further experimental work is needed to address the phase composition of the phosphate ceramics produced as a function of phosphorus mole fraction of the cation-loaded ZrBTP-x phase.

4. DISCUSSION

It is well-known that most coordination polymers prepared from tetravalent cations are highly insoluble such that rapid precipitation occurs when solutions of the metal and ligand are combined. Thus, recrystallization is usually impossible, and special techniques have had to be developed to overcome this problem.[56] One such technique involves the layering in a small vial of two solutions on top of each other, one containing the metal and the other the ligand. Slow diffusion of one solution into the other allows slow crystallization to occur. Although this technique has been used in certain cases to produce very small quantities of materials suitable for single-crystal X-ray diffraction, it is not suitable for producing sufficient material for evaluating properties or for producing the quantities of materials necessary for real-world applications or even to enable sorption studies to be undertaken.

To the author's knowledge there have been only three reports of crystalline MOFs prepared from BTP. These have involved the following metals including Cu,[45] Pb,[57] and Fe.[58] However, X-ray amorphous Zr phosphonates based on other phosphonate ligands have been reported, and the extraction of heavy elements such as Hg, Cd, Cu, and Pb has been investigated[59] including by the author and his colleagues.[40,41]

Using the rigid BTP ligand herein it has been possible to prepare ZrBTP compounds with X-ray powder patterns ranging from those indicative of poorly ordered nanocrystalline materials to those indicative of extremely well-ordered nanocrystalline materials depending on whether or not a mineralizing agent such as HF is used. Not surprisingly, it has been found here that the most effective ZrBTP extractants are the least crystalline Gen I materials with x in the range 0.7−0.9 having particle diameters ∼30 nm and a decrease in the surface area from 500 to 30 m^2/g. That said, the somewhat more crystalline mixed-phase Gen II materials prepared using HF and having slightly larger particle sizes and surface areas exceeding 50 m^2/g, also appear to function reasonably well. In contrast, the highly crystalline Gen III materials showed relatively low sorption capacities. Microanalytical measurement and other data have confirmed that the very fine-grained Gen I materials are obtained with the same overall stoichiometry of the reaction mixture. From the XRD results it appears that the poorly crystalline Gen I materials have the incipient structure of the phases that subsequently become more crystalline as HF is included as a mineralizing agent. Unfortunately, the multiphase nature of the crystalline phases obtained has precluded crystal structure solution of these materials within the field of compositional space being investigated. Clearly, other techniques will need to be employed to prepare more crystalline materials suitable for single-crystal or ab initio structure determination from powders.

Although the nanocrystalline Gen I materials appear to have similar structural motifs to the microcrystalline Gen II and III phases it would appear that particle packing as well as phosphonic acid packing within and between nanoparticles is high.

Various options could be considered for the structural motif of the Gen I materials. One possibility could be that the materials are simply nanoparticles of zirconia or oxyhydroxides capped with polyphosphonates. However, zirconia nanoparticles can be ruled out, since neither XRD or FTIR data support this hypothesis. Polyphosphonate-capped, poorly crystalline zirconium oxyhydroxide can also be discounted if the resemblance to the crystalline phases that are produced on addition of HF is accepted and considering that these phases do no match any known material.

Regardless of the particle sizes and the phases involved in the Gen I−III materials, similar cation selectivities are observed for all samples. From the similarity in the selectivity of all of the

DOI: 10.1021/acs.inorgchem.6b00954
Inorg. Chem. XXXX, XXX, XXX−XXX

ZrBTP-x materials and the X-ray amorphous materials previously prepared from ATMP[40] and zoledronic acid,[41] it can be concluded that sorption properties of the zirconium polyphosphonates are primarily determined by the acidity of the phosphonate groups and are little influenced by the detailed architecture of the coordination polymer. Indeed, in the case of the previously reported Zr(IV)-zoledronate materials, perturbations of the P−O stretching frequencies in the FTIR spectra after sorption of Th^{4+} convincingly linked the sorption properties to the phosphonate groups. Similar observations of modulated phosphonate group stretching frequencies have also been made for the present materials (see Figure S11 of Supporting Information section). The existence of bands at 1385 cm^{-1} in the FTIR spectra of Th^{4+} saturated samples also suggests that the nitrate anion remains in the coordination sphere during sorption. In addition, it has also been shown that progressive replacement of one (ZrBDP-x) and two phosphonates (ZrBMP-x) of the benzene ring by carboxylate does little to modify the underlying selectivity and only serves to reduce capacity. Since the carboxylate group appears not to modify to any great extent the selectivity it might be surmised that the carboxylate group is involved in framework building but not cation binding. This once again implicates phosphonate groups in cation binding.

One potentially very important result of this study that requires further investigation is the tendency of the ZrBTP-x materials to display a much higher capacity for the extraction of heavy lanthanides such as Dy^{3+} and Ho^{3+} compared with light lanthanides at high equilibrium cation concentrations (Figure 15). At high HNO_3 concentrations the increase in selectivity and hence extractability as a function of lanthanide atomic number is particularly pronounced. Such data suggest that in a column configuration, the present materials should show excellent prospects for the selective extraction of these two industrially important lanthanides from complex solutions including those containing other lanthanides. Studies of the column performance of granulated versions of the ZrBTP materials are ongoing and will be reported in due course.

In studies of lanthanide adsorption on different aluminosilicates including zeolites[60] and clay minerals[61] K_d values exhibit a general overall increase across the lanthanide series. Superimposed on this overall increase in K_d with decreasing ionic radius is observed a dip at Nd^{3+}, Gd^{3+}, and Er^{3+} corresponding to the one-fourth, one-half, and three-fourths filled 4f subshell. This has been dubbed a "tetrad effect" and consists of a subtle decrease in K_d every fourth element in the lanthanide series. Such an effect was best accounted for theoretically by Kawabe in 1992.[62] Since the sorption data presented in this study have not included all lanthanides, it is not possible to categorically rule out such a subtle effect here. However, at the ionic strengths investigated a progressive increase in K_d values across the lanthanide series has been clearly observed, and separation factors between heavy and light lanthanides range from 2 to 10. At high ionic strengths and lower HNO_3 concentrations a more abrupt discontinuity in the adsorption of Dy^{3+} and Ho^{3+} compared to the other lanthanides was observed. Under such conditions, separation factors between Dy and Ho and other lanthanides ($K_{d(Dy)}/K_{d(M)}$) are in the range of 4−6 and would seem to be quite useful in terms of the separation of these two lanthanides. In addition we observed very rapid kinetics for the Gen I materials with maximum sorption occurring within seconds to minutes, which is for practical purposes instantaneous.

While most coordination polymers/MOFs that have been reported to date are macroscopic crystalline materials generally having high surface areas, examples of nanoparticulate and X-ray amorphous MOFs have been reported. For instance, Oh et al.[28] reported the solvent-initiated spontaneous formation of nanoparticulate coordination polymers based on Schiff bases. It has also been demonstrated that crystalline zeolite imidazolate frameworks (ZIFs) such as ZIF-8 can be amorphized relatively easily via the application of pressure to yield X-ray amorphous materials with similar short-range order to the crystalline counterparts. Such amorphous ZIFs can be advantageous from an applications point of view. The idea has been ventured that crystalline ZIFs can be used for the incorporation of guest molecules such as CO_2 and I_2 and that subsequent collapse of the framework through the application of pressure can be used to entrap these molecules.[63]

This is related to the thrust of our work over more than a decade during which we have focused on the development of materials for the selective extraction of ionic species and the subsequent conversion of the nanostructured adsorbent into a crystalline phase in which the extracted species is irreversibly bound. In this regard our data show that the lanthanide- and actinide-loaded adsorbents are always converted to Zr pyrophosphate structures (ZrP_2O_7). As phosphate ceramics are generally regarded as being very insoluble many studies have addressed the use of phosphate ceramics as matrices for the immobilization of radioactive actinide and fission product elements. In this regard Itoh et al.[64] have shown that even Cs can be converted to highly stable phosphate ceramics at 700 °C having Cs leach rates less than 1×10^{-11} g cm^{-2} day^{-1} in 0.1 mol/L HCl at 100 °C far exceeding those of borosilicate glass.

ZrP_2O_7 is one of the most widely studied members of the pseudo cubic $A^{IV}M^{V}{}_2O_7$ extensive family of materials (M = P, V, As) in which a great variety of ions can be found, in particular, that occupy the A site (Si, Ge, Sn, Pb, Ti, Zr, Hf, Mo, W, Re, Ce, U), while the M site can accommodate elements such as P, V, and As.[65]

The ideal (usually high-temperature) parent structure (space group symmetry $Pa31$, $Z'' = 4$) is built of corner-connected AO_6 octahedra and nominally linear M_2O_7 (pyrophosphate, pyrovanadate, or pyroarsenate) units (in turn built of two corner-connected MO_4 tetrahedra), as shown in (Figure S9 of the Supporting Information). Thus, it is obvious that the structure is quite versatile in terms of the compositions.

The present study explored only the phosphorus-rich region of the Zr−P−F phase diagram. Further work is needed to explore the compositional field in greater detail and to focus on the crystallization of single-phase materials that are amenable to structure solution by either single-crystal diffraction or ab initio methods and more precise determination of structure−function relationships.

The classical extractants for lanthanide separations include the likes of alkyl phosphoric and phosphonic acids (e.g., 2-ethylhexyl phosphoric acid, HDEHP), amines (e.g., Cyannex 301), carboxylic acids (e.g., Versatic 10), and so forth.[4] Each of these have been investigated extensively and have shown efficiency in both intralanthide and actinide−lanthanide separations in both solvent extraction and extraction chromatographic form. Recently, Wei et al.[66] investigated HDEHP-based extraction chromatography in which the support phase comprised polymer-loaded silica spheres. These materials were relatively ineffective at HNO_3 concentrations greater than one giving K_d values less than 100 for trivalent Ce, Gd, Eu,

DOI: 10.1021/acs.inorgchem.6b00954
Inorg. Chem. XXXX, XXX, XXX−XXX

and Am. The relatively small differneces in K_d between lanthanides and the actinide suggested that a practical intralanthanide or lanthanide−actinide would not be achievable.

On the other hand Silbernagel[67] recently reported the preparation of zirconium phosphate-phosphonates that have shown interesting lanthanide extraction properties. The Zr(IV)-BTP hybrids of the present study seem to significantly outperform those materials, as efficient extractions can be achieved even up to 4 M HNO_3. These are acid concentrations relevant to nuclear fuel reprocessing raffinates as well as in mining liquors.

The present ZrBTP-x materials therefore would seem to offer interesting prospects for lanthanide-major actinide and lanthanide-minor actinide separations especially at the back-end of the nuclear fuel cycle. Also extremely relevant is the data presented that indicated that intralanthanide separations can be accomplished with the present materials. The ability to separate a particular lanthanide, especially a heavy lanthanide from within the series using an operationally simple approach with few unit operations, might prove to be invaluable, as expanded technological applications result in increased demand for heavy lanthanides, in particular.[68]

We are presently focusing on the column deployment of the nanostructured ZrBTP-x materials especially in the granular form utilizing a polyacrylonitrile binding matrix as well as better defining the chemical stability of the phosphate ceramics derived through thermal treatment of the lanthanide and actinide-loaded nanostructured Zr phosphonates.

Although the most effective materials prepared here are nanometer-sized particles that do not lend themselves easily to use as stationary phases in packed columns, we show here that good initial results can be achieved through the incorporation of the ZrBTP-x materials in sub-millimeter size polyacrylonitrile matrices for use in columns. This work will be reported in due course.

5. CONCLUSIONS

Solid extractants consisting of poorly crystalline Zr(IV)-coordination polymers based on BTP and carboxylate-substituted derivatives have been prepared. The use of HF as a mineralizer resulted in crystalline mixed-phase compounds whose structure could not be resolved. Of the materials studied, the poorly crystalline ZrBTP-x phases prepared in the absence of fluoride showed superior performance in the extraction of trivalent lanthanides and tetravalent Th even in greater than 3 M HNO_3. Under such highly acidic conditions, the compounds remained stable and displayed enhanced selectivity for heavy lanthanides, suggesting that they might be useful for actual applications. In addition to excellent selectivity for the mentioned trivalent elements the ZrBTP-x compounds showed extremely fast kinetics and good capacities. It remains to be seen if appropriate choice of conditions could result in materials suitable for the extraction of trivalent actinides from radio lanthanides. Work addressing column dynamics of granulated materials and the extraction of radiolanthanides and actinides from Purex-type raffinates is underway. Thermal treatment of the lanthanide and Th-loaded extractants results in formation of highly crystalline pyrophosphates with the general formula $A^{IV}P_2O_7$ and where Zr, Th, and the lanthanides occupy the A site. Such materials are expected to be highly insoluble and therefore suitable for radioactive waste repository disposition after suitable conditioning.

■ ASSOCIATED CONTENT

Supporting Information

The Supporting Information is available free of charge on the ACS Publications website at DOI: 10.1021/acs.inorgchem.6b00954.

FTIR data, additional XRD patterns, small-angle X-ray scattering data, polyhedral structure representations (PDF)

■ AUTHOR INFORMATION

Corresponding Author

*E-mail: vluca@cnea.gov.ar.

Notes

The authors declare no competing financial interest.

■ ACKNOWLEDGMENTS

The authors would like express their sincere appreciation to S. Maynadie of the Institut de Chimie Séparative de Marcoule for acquisition of the ^{31}P MAS NMR data. Gratitude is due to Antonio Ciagla for assistance with some of the adsorption experiments. Major funding for this work was provided by the Comisión Nacional de Energía Atómica.

■ REFERENCES

(1) Davidson, D.; Hunter, I. Benefits of an Integrated Fuel Cycle on Repository Effective Capacity. *Waste Management Symposium—Global Accomplishments in Environmental and Radioactive Waste Management;* Tucson, AZ, 2006.

(2) Kessler, G. *Sustainable and Safe Nuclear Fission Energy—Technology and Safety of Fast and Thermal Nuclear Reactors;* Springer: Heidelberg, Germany, 2012; p 243.

(3) Malmbeck, R.; Nourry, C.; Ougier, M.; Soucek, P.; Glatz, J. P.; Kato, T.; Koyama, T. *Energy Procedia* **2011**, *7*, 93−102.

(4) Xie, F.; Zhang, T. A.; Dreisinger, D.; Doyle, F. *Miner. Eng.* **2014**, *56*, 10−28.

(5) Wood, S. A. *Chem. Geol.* **1990**, *82*, 159−186.

(6) Gelis, A. V.; Vandegrift, G. F.; Bakel, A.; Bowers, D. L.; Hebden, A. S.; Pereira, C.; Regalbuto, M. *Radiochim. Acta* **2009**, *97*, 231−232.

(7) Lumetta, G. J.; Gelis, A. V.; Braley, J. C.; Carter, J. C.; Pittman, J. W.; Warner, M. G.; Vandegrift, G. F. *Solvent Extr. Ion Exch.* **2013**, *31*, 223−236.

(8) Mincher, B. J.; Schmitt, N. C.; Case, M. E. *Solvent Extr. Ion Exch.* **2011**, *29*, 247−259.

(9) Nash, K. L. *J. Alloys Compd.* **1997**, *249*, 33−40.

(10) Zheng, Z.; Philip, C. V.; Anthony, R. G.; Krumhansl, J. L.; Trudell, D. E.; Miller, J. E. *Ind. Eng. Chem. Res.* **1996**, *35*, 4246−4256.

(11) Zheng, Z.; Gu, D.; Anthony, R. G.; Klavetter, E. *Ind. Eng. Chem. Res.* **1995**, *34*, 2142−2147.

(12) Feng, X.; Fryxell, G. E.; Wang, L.-Q.; Kim, A. Y.; Liu, J.; Kemner, K. M. *Science* **1997**, *276*, 923−926.

(13) Griffith, C. S.; De Los Reyes, M.; Scales, N.; Hanna, J. V.; Luca, V. *ACS Appl. Mater. Interfaces* **2010**, *2*, 3436−3446.

(14) Luca, V.; Bertram, W. K.; Widjaja, J.; Mitchell, D. R. G.; Griffith, C. S.; Drabarek, E. *Microporous Mesoporous Mater.* **2007**, *103*, 123−133.

(15) Sizgek, G. D.; Sizgek, E.; Griffith, C. S.; Luca, V. *Langmuir* **2008**, *24*, 12323−12330.

(16) Sizgek, G. D.; Griffith, C. S.; Sizgek, E.; Luca, V. *Langmuir* **2009**, *25*, 11874−11882.

(17) Fryxell, G. E.; Wu, H.; Lin, Y.; Shaw, W. J.; Birnbaum, J. C.; Linehan, J. C.; Nie, Z.; Kemner, K.; Kelly, S. *J. Mater. Chem.* **2004**, *14*, 3356−3363.

(18) Fryxell, G. E.; Lin, Y.; Fiskum, S.; Birnbaum, J. C.; Wu, H.; Kemner, K.; Kelly, S. *Environ. Sci. Technol.* **2005**, *39*, 1324−1331.

DOI: 10.1021/acs.inorgchem.6b00954
Inorg. Chem. XXXX, XXX, XXX−XXX

(19) Florek, J.; Chalifour, F.; Bilodeau, F.; Lariviére, D.; Kleitz, F. *Adv. Funct. Mater.* **2014**, *24*, 2668−2676.
(20) Shusterman, J. A.; Mason, H. E.; Bowers, J.; Bruchet, A.; Uribe, E. C.; Kersting, A. B.; Nitsche, H. *ACS Appl. Mater. Interfaces* **2015**, *7*, 20591−20599.
(21) Zhu, Y.-P.; Yuan, Z.-Y. *Mesoporous Organic-Inorganic Non-Siliceous Hybrid Materials - Basic Principles and Promising Multi-functionality;* Springer: Heidelberg, Germany, 2015.
(22) Braun, T.; Ghersini, G. *Extraction Chromatography;* Elsevier: Amsterdam, 1975.
(23) Zhang, A.; Wei, Y.; Kumagai, M. *J. Radioanal. Nucl. Chem.* **2005**, *265*, 409−417.
(24) Horwitz, E. P.; Chiarizia, R.; Dietz, M. L.; Diamond, H.; Nelson, D. M. *Anal. Chim. Acta* **1993**, *281*, 361−72.
(25) Horwitz, E. P.; Dietz, M. L.; Nelson, D. M.; Larosa, J. J.; Fairman, W. D. *Anal. Chim. Acta* **1990**, *238*, 263−271.
(26) Mokhodoeva, O. B.; Myasoedova, G. V.; Zakharchenko, E. A. *Radiochemistry* **2011**, *53*, 35−43.
(27) Hong, M.-C.; Chen, L. *Extraction Chromatography;* Wiley, 2009.
(28) Oh, M.; Mirkin, C. A. *Nature* **2005**, *438*, 651−654.
(29) Poojary, D. M.; Vermeulen, L. A.; Vicenzi, E.; Clearfield, A.; Thompson, M. E. *Chem. Mater.* **1994**, *6*, 1845−1849.
(30) Alberti, G.; Casciola, M.; Costantino, U.; Vivani, R. *Adv. Mater.* **1996**, *8*, 291−303.
(31) Kitagawa, S.; Matsuda, R. *Coord. Chem. Rev.* **2007**, *251*, 2490−2509.
(32) Cahill, R.; Shpeizer, B.; Peng, G. Z.; Bortun, L.; Clearfield, A. *Separation of f Elements, Proc. Am. Chem. Soc. Symp.* **1995**, 165−76.
(33) Burns, J. D.; Shehee, T. C.; Clearfield, A.; Hobbs, D. T. *Anal. Chem.* **2012**, *84*, 6930−6932.
(34) Burns, J. D.; Clearfield, A.; Borkowski, M.; Reed, D. T. *Radiochim. Acta* **2012**, *100*, 381−387.
(35) Amicangelo, J. C.; Leenstra, W. R. *Inorg. Chem.* **2005**, *44*, 2067−2073.
(36) Costantino, F.; Donnadio, A.; Casciola, M. *Inorg. Chem.* **2012**, *51*, 6992−7000.
(37) Leenstra, W. R.; Amicangelo, J. C. *Inorg. Chem.* **1998**, *37*, 5317−5323.
(38) Lin, X.-Z.; Yuan, Z.-Y. *Eur. J. Inorg. Chem.* **2012**, *2012*, 2661−2664.
(39) Carboni, M.; Abney, C. W.; Liu, S.; Lin, W. *Chem. Sci.* **2013**, *4*, 2396−2402.
(40) Veliscek-Carolan, J.; Hanley, T. L.; Luca, V. *Sep. Purif. Technol.* **2014**, *129*, 150−158.
(41) Luca, V.; Hanna, J. V. *Hydrometallurgy* **2015**, *154*, 118−128.
(42) Zhu, Z.; Pranolo, Y.; Cheng, C. Y. *Miner. Eng.* **2015**, *77*, 185−196.
(43) Jenkins, I. L. *Hydrometallurgy* **1979**, *5*, 1−13.
(44) Su, Y.; Balmer, M. L.; Wang, L.; Bunker, B. C.; Nyman, M.; Nenoff, T.; Navrotsky, A. *MRS Online Proc. Libr.* **1999**, *556*, 77−84.
(45) Kong, D.; Zon, J.; McBee, J.; Clearfield, A. *Inorg. Chem.* **2006**, *45*, 977−986.
(46) Ho, Y.-S. *J. Hazard. Mater.* **2006**, *136*, 681−689.
(47) Ho, Y. S.; McKay, G. *Adsorpt. Sci. Technol.* **2002**, *20*, 797−815.
(48) Fernandez Lopez, E.; Sanchez Escribano, V.; Panizza, M.; Carnasciali, M. M.; Busca, G. *J. Mater. Chem.* **2001**, *11*, 1891−1897.
(49) Brunet, E.; Cerro, C.; Juanes, O.; Rodriguez-Ubis, J.; Clearfield, A. *J. Mater. Sci.* **2008**, *43*, 1155−1158.
(50) Josse, S.; Faucheux, C.; Soueidan, A.; Grimandi, G.; Massiot, D.; Alonso, B.; Janvier, P.; Laib, S.; Pilet, P.; Gauthier, O.; Daculsi, G.; Guicheux, J. m.; Bujoli, B.; Bouler, J.-M. *Biomaterials* **2005**, *26*, 2073−2080.
(51) Hanna, J. V.; Smith, M. E. *Solid State Nucl. Magn. Reson.* **2010**, *38*, 1−18.
(52) Gómez-Alcantara, M. d. M.; Cabeza, A.; Moreno-Real, L.; Aranda, M. A. G.; Clearfield, A. *Microporous Mesoporous Mater.* **2006**, *88*, 293−303.
(53) Kunz, W. *Specific Ion Effects;* World Scientific, 2009.
(54) Limousin, G.; Gaudet, J.-P.; Charlet, L.; Szenknect, S.; Barthes, V.; Krimissa, M. *Appl. Geochem.* **2007**, *22*, 249−275.
(55) Chiarizia, R.; Mcalister, D. R.; Herlinger, A. W. *Sep. Sci. Technol.* **2005**, *40*, 69−90.
(56) Batten, S. R.; Neville, S. M.; Turner, D. R. *Coordination Polymers - Design, Analysis and Application;* RSC Publishing, 2009; p 10.
(57) Tang, S.-F.; Lv, X.-X.; Li, L.-J.; Wang, C.; Zhao, X.-B. *Inorg. Chem. Commun.* **2014**, *39*, 51−55.
(58) Pramanik, M.; Bhaumik, A. *Chem. - Eur. J.* **2013**, *19*, 8507−8514.
(59) Shah, B.; Chudasam, U. *Desalin. Water Treat.* **2012**, *38*, 276−284.
(60) Gladysz-Plaska, A.; Majdan, M.; Pikus, S.; Lewandowski, W. *J. Colloid Interface Sci.* **2007**, *313*, 97−107.
(61) Coppin, F.; Berger, G.; Bauer, A.; Castet, S.; Loubet, M. *Chem. Geol.* **2002**, *182*, 57−68.
(62) Kawabe, I. *Geochem. J.* **1992**, *26*, 309−335.
(63) Chapman, K. W.; Sava, D. F.; Halder, G. J.; Chupas, P. J.; Nenoff, T. M. *J. Am. Chem. Soc.* **2011**, *133*, 18583−18585.
(64) Itoh, K.; Nakayama, S. *J. Mater. Sci.* **2002**, *37*, 1701−1704.
(65) Withers, R. L.; Tabira, Y.; Evans, J. S. O.; King, I. J.; Sleight, A. W. *J. Solid State Chem.* **2001**, *157*, 186−192.
(66) Wei, W.; Kumagai, M.; Takashima, Y.; Modolo, G.; Odoj, R. *Nucl. Technol.* **2000**, *132*, 413−423.
(67) Silbernagel, R.; Martin, C. H.; Clearfield, A. *Inorg. Chem.* **2016**, *55*, 1651−1656.
(68) Hatch, G. P. *Elements* **2012**, *8*, 341−346.

DOI: 10.1021/acs.inorgchem.6b00954
Inorg. Chem. XXXX, XXX, XXX−XXX